

# 1 **Biallelic *BORCS8* variants cause an infantile-onset** 2 **neurodegenerative disorder with altered lysosome dynamics**

3 Raffaella De Pace,<sup>1,†</sup> Reza Maroofian,<sup>2,†</sup> Adeline Paimboeuf,<sup>3,†</sup> Mina Zamani,<sup>4,5</sup> Maha S. Zaki,<sup>6</sup>  
4 Saeid Sadeghian,<sup>7</sup> Reza Azizimalamiri,<sup>7</sup> Hamid Galehdari,<sup>4</sup> Jawaher Zeighami,<sup>5</sup> Chad D.  
5 Williamson,<sup>1</sup> Emily Fleming,<sup>8</sup> Dihong Zhou,<sup>8,9</sup> Jennifer L. Gannon,<sup>9,10</sup> Isabelle Thiffault,<sup>8,11</sup>  
6 Emmanuel Roze,<sup>12</sup> Mohnish Suri,<sup>13</sup> Giovanni Zifarelli,<sup>14</sup> Peter Bauer,<sup>14</sup> Henry Houlden,<sup>2</sup>  
7 Mariasavina Severino,<sup>15</sup> Shunmoogum A. Patten,<sup>3,16</sup> Emily Farrow<sup>8,17</sup> and Juan S. Bonifacino<sup>1</sup>

8 † **These authors contributed equally to this work.**

## 9 **Abstract**

10 BLOC-One-Related Complex (BORC) is a multiprotein complex composed of eight subunits  
11 named BORCS1-8. BORC associates with the cytosolic face of lysosomes, where it sequentially  
12 recruits the small GTPase ARL8 and kinesin-1 and -3 microtubule motors to promote  
13 anterograde transport of lysosomes toward the peripheral cytoplasm in non-neuronal cells and  
14 the distal axon in neurons. The physiological and pathological importance of BORC in humans,  
15 however, remains to be determined. Here, we report the identification of compound  
16 heterozygous variants [missense c.85T>C (p.Ser29Pro) and frameshift c.71-75dupTGGCC  
17 (p.Asn26Trpfs\*51)] and homozygous variants [missense c.196A>C (p.Thr66Pro) and c.124T>C  
18 (p.Ser42Pro)] in *BORCS8* in five children with a severe early-infantile neurodegenerative  
19 disorder from three unrelated families. The children exhibit global developmental delay, severe-  
20 to-profound intellectual disability, hypotonia, limb spasticity, muscle wasting, dysmorphic  
21 facies, optic atrophy, leuko-axonopathy with hypomyelination, and neurodegenerative features  
22 with prevalent supratentorial involvement.

23 Cellular studies using a heterologous transfection system show that the *BORCS8* missense  
24 variants p.Ser29Pro, p.Ser42Pro and p.Thr66Pro are expressed at normal levels but exhibit  
25 reduced assembly with other BORC subunits and reduced ability to drive lysosome distribution  
26 toward the cell periphery. The *BORCS8* frameshift variant p.Asn26Trpfs\*51, on the other hand,  
27 is expressed at lower levels and is completely incapable of assembling with other BORC  
28 subunits and promoting lysosome distribution toward the cell periphery.

1 Therefore, all the *BORCS8* variants are partial or total loss-of-function alleles and are thus likely  
2 pathogenic. Knockout of the orthologous *borcs8* in zebrafish causes decreased brain and eye  
3 size, neuromuscular anomalies and impaired locomotion, recapitulating some of the key traits of  
4 the human disease.

5 These findings thus identify *BORCS8* as a novel genetic locus for an early-infantile  
6 neurodegenerative disorder and highlight the critical importance of BORG and lysosome  
7 dynamics for the development and function of the central nervous system.

8

9 **Author affiliations:**

10 1 Neurosciences and Cellular and Structural Biology Division, Eunice Kennedy Shiver National  
11 Institute of Child Health and Human Development, National Institutes of Health, Bethesda, MD  
12 20892, USA

13 2 UCL Queen Square Institute of Neurology, London WC1N 3BG, UK

14 3 INRS – Centre Armand Frappier Santé Biotechnologie, Laval, QC H7V 1B7, Canada

15 4 Department of Biology, Faculty of Science, Shahid Chamran University of Ahvaz, Ahvaz,  
16 83151-61355, Iran

17 5 Narges Medical Genetics and Prenatal Diagnosis Laboratory, Kianpars, Ahvaz, 61556-89467,  
18 Iran

19 6 Human Genetics and Genome Research Division, Clinical Genetics Department, National  
20 Research Centre, Cairo, 12622, Egypt

21 7 Department of Pediatric Neurology, Golestan Medical, Educational, and Research Center,  
22 Ahvaz Jundishapur University of Medical Sciences, Ahvaz, 61357-33184, Iran

23 8 Department of Genetics, Children’s Mercy Kansas City, Kansas City, MO 64108, USA

24 9 Department of Pediatrics, University of Missouri-Kansas City School of Medicine, Kansas  
25 City, MO 64108, USA

26 10 Division of Clinical Genetics, Children’s Mercy Kansas City, Kansas City, MO 64108, USA

27 11 Department of Pathology, Children’s Mercy Kansas City, Kansas City, MO 64108, USA

1 12 Sorbonne Université, CNRS, INSERM, Institut du Cerveau (ICM), and Assistance Publique-  
2 Hôpitaux de Paris, Hôpital de la Pitié-Salpêtrière, Paris, 75013, France

3 13 Nottingham Clinical Genetics Service, Nottingham University Hospitals NHS Trust, City  
4 Hospital Campus, Nottingham, NG5 1PB, UK

5 14 CENTOGENE GmbH, Am Strande 7, 18055 Rostock, Germany

6 15 Neuroradiology Unit, IRCCS Istituto Giannina Gaslini, Genoa, 16147, Italy

7 16 Département de Neurosciences, Université de Montréal, QC H3C 3J7, Canada

8 17 Genomic Medicine Center, Children's Mercy Kansas City, Kansas City, MO 64108, USA

9

10 Correspondence to: Dr Juan S. Bonifacino

11 Division of Neurosciences and Cellular and Structural Biology Division, *Eunice Kennedy*  
12 *Shriver* National Institute of Child Health and Human Development (NICHD), National  
13 Institutes of Health (NIH), Building 35, Room 2F-226, 35A Convent Drive, MSC 3758,  
14 Bethesda, MD 20892-3758, USA

15 E-mail: [juan.bonifacino@nih.gov](mailto:juan.bonifacino@nih.gov)

16

17 Correspondence may also be addressed to: Dr Emily Farrow

18 Department of Genetics, Children's Mercy Hospital, 2401 Gilham Road, 3rd Floor East CMRI,  
19 3902.15, Kansas City, MO 64108, USA

20 E-mail: [egfarrow@cmh.edu](mailto:egfarrow@cmh.edu)

21

22 Dr Shunmoogum A. Patten

23 INRS – Centre Armand Frappier Santé Biotechnologie, 531 Boul. des Prairies, Laval, QC, H7V  
24 1B7, Canada

25 E-mail: [Kessen.Patten@inrs.ca](mailto:Kessen.Patten@inrs.ca)

26

1 **Running title:** *BORCS8* variants cause neurological disease

2 **Keywords:** lysosomes; neurodevelopmental disorder; neurodegeneration; leukodystrophy;  
3 hereditary spastic paraplegia

4 **Abbreviations:** ARL8, ADP-ribosylation factor like 8; ABR, auditory brainstem response;  
5 BORG, BLOC-1-related complex; BSA, bovine serum albumin; CRISPR, clustered regularly  
6 interspaced short palindromic repeats; DD, developmental disability; dpf, days postfertilization;  
7 gRNA, guide RNA; HA, haemagglutinin; ICV, intracerebroventricular; ID, intellectual  
8 disability; KLC1, kinesin light chain 1; KO, knock out; LAMP1, lysosomal associated  
9 membrane protein 1; LSB, Laemmli sample buffer; OFC, occipitofrontal circumference; RNPs,  
10 ribonucleoproteins; WT, wild type

11

## 12 **Introduction**

13 BLOC-one-related complex (BORG) is a ubiquitously expressed protein complex composed of  
14 eight subunits named BORCS1-8.<sup>1</sup> BORG associates with the cytosolic face of lysosomal and  
15 late endosomal organelles (herein collectively referred to as “lysosomes”) at least in part through  
16 a myristoyl group at the *N*-terminus of BORCS5<sup>1</sup> and an interaction of BORCS6 with the  
17 regulator complex.<sup>1,2,3,4</sup> BORG then promotes the recruitment of the small GTPase ARL8 (which  
18 in mammals exists as two paralogs, ARL8A and ARL8B)<sup>5</sup> to lysosomes.<sup>1</sup> In turn, ARL8 recruits  
19 the motor proteins kinesin-1 (via the adaptor protein PLEKHM2/SKIP)<sup>6</sup> and kinesin-3  
20 (directly).<sup>7</sup> BORG/ARL8-mediated coupling to these kinesins enables anterograde transport of  
21 lysosomes along microtubule tracks toward the peripheral cytoplasm in non-polarized cells<sup>1,6,8</sup>,  
22 and the distal axon in neurons.<sup>9,10,11</sup> The ability of lysosomes to move within the cytoplasm is  
23 critical for many cellular functions, including cell adhesion and migration,<sup>1,12</sup> invasive cancer  
24 growth,<sup>13</sup> plasma membrane repair,<sup>14</sup> metabolic signaling<sup>15,16</sup> and maintenance of axonal  
25 health.<sup>9,11</sup>

26 Homozygous ablation of the *Borcs5*<sup>9</sup> or *Borcs7*<sup>11</sup> genes in mice (*Borcs5*<sup>-/-</sup> or *Borcs7*<sup>-/-</sup>  
27 mice, respectively) causes neonatal lethality due to suffocation and/or failure to feed in the first  
28 hours of life. Homozygous mice bearing a spontaneous truncating mutation (p.Q87X) in *Borcs7*  
29 (*Borcs7*<sup>Q87X/Q87X</sup>) are viable, but develop progressive axonal dystrophy and impairment of motor

1 function.<sup>11</sup> Analyses of cortical and hippocampal neurons cultured from *Borcs5*<sup>-/-</sup>, *Borcs7*<sup>-/-</sup> or  
2 *Borcs7*<sup>Q87X/Q87X</sup> E15-18 embryos revealed clustering of lysosomes in the soma and their depletion  
3 from the axon.<sup>9,11</sup> Moreover, immunohistochemical analyses of tissues from *Borcs5*<sup>-/-</sup> mice  
4 showed reduced staining for lysosomes in axon-enriched regions of the corpus callosum and  
5 molecular layer of the hippocampus, and at neuromuscular junctions in the diaphragm.<sup>9</sup> Finally,  
6 axons in the phrenic and spinal nerves were found to contain numerous eosinophilic dystrophic  
7 bodies or spheroids indicative of degeneration.<sup>9</sup> These studies thus revealed that, despite the  
8 ubiquitous presence of BORC in many cells and tissues, the pathologic consequences of its  
9 deficiency are mainly manifested in the CNS.

10 To date, little is known about the importance of BORC in human physiology and  
11 pathology. A study involving whole-exome sequencing in 31 mostly consanguineous Arab  
12 families with neurologic disease identified a c203-1G>T biallelic splice variant in *BORCS5*  
13 (referred to as *LOH12CRI* in that study) in a patient featuring autosomal recessive  
14 developmental delay, microcephaly, seizures, cortical malformation, polymicrogyria and  
15 agenesis of the corpus callosum.<sup>17</sup> However, this study did not provide a detailed clinical  
16 characterization of the patient nor a functional analysis of the variant protein.

17 Here, we report five children from three independent families presenting with a severe  
18 neurodegenerative disorder associated with biallelic variants in *BORCS8*. The children exhibit  
19 global developmental delay, intellectual disability, hypotonia, spasticity, muscle wasting,  
20 dysmorphic facies, optic atrophy, leuko-axonopathy with hypomyelination, and  
21 neurodegenerative features with prevalent supratentorial involvement. Cellular studies using a  
22 heterologous transfection system show that the variant proteins exhibit reduced assembly with  
23 other BORC subunits and reduced ability to promote lysosome distribution toward the cell  
24 periphery. Moreover, *borcs8*-KO zebrafish display neurodevelopmental defects, recapitulating  
25 some of the key traits of the human disease. These studies thus identify *BORCS8* as a novel gene  
26 locus for an early-infantile neurodegenerative disorder and demonstrate the critical importance of  
27 BORC for the development and function of the CNS.

28

29

# 1 **Material and methods**

## 2 **Patient ascertainment and clinical and molecular studies**

3  
4 Three unrelated families of European-American (FI), Iranian-Arab (FII) and Egyptian ancestry  
5 (FIII) were recruited and studied (Fig. 1A and Supplementary Fig. 1). The study was approved  
6 by the institutional ethics committees of the Children's Mercy Kansas City Hospital (Children's  
7 Mercy IRB# 11120514) and University College London (IRB# 310045/1571740/37/598), and  
8 written informed consent was obtained from all three families in accordance with the Declaration  
9 of Helsinki. Deidentified skin fibroblasts from the patients and the mother of the European-  
10 American family were shared with the National Institutes of Health (NIH) laboratory for  
11 research purposes. Skin fibroblasts from a healthy individual (85E0344) and from an SPG50  
12 patient that carries pathogenic mutations in the *AP4MI* and *ATS* genes (87RD39)<sup>18,19</sup> were used  
13 as controls. Detailed clinical features, photos, videos, brain MRI imaging, family history and  
14 clinical notes were obtained from all affected individuals and reviewed by a group of clinical  
15 geneticists, dysmorphologists and pediatric neurologists. Brain MRIs were reviewed by an  
16 experienced pediatric neuroradiologist. Genome, exome, and Sanger sequencing were performed  
17 independently at three different research and clinical laboratories as described previously.<sup>20,21,22</sup>

## 18 19 **Culture and transfection of human cells lines**

20 HEK293T cells, HeLa cells and human skin fibroblasts were cultured in DMEM (Quality  
21 Biological), supplemented with 2 mM L-glutamine (GIBCO), 10% fetal bovine serum (GIBCO),  
22 100 U/ml penicillin-streptomycin (GIBCO) (complete DMEM) in a 37°C incubator (5% CO<sub>2</sub>,  
23 95% air). HeLa cells grown on 6-well plates were transiently transfected with 0.8 µg plasmid  
24 DNA using 2 µl Lipofectamine 2000 (Invitrogen), according to the manufacturer's instructions.  
25 Approximately 24 h after transfection, cells were replated onto 12-mm coverslips coated with  
26 collagen. Cells were then cultured for an additional 24 h before fixation and immunofluorescent  
27 labeling. This longer transfection period was necessary for rescue of the BORC phenotype. For  
28 the co-immunoprecipitation and MG132 treatment experiments shown in Fig. 4, HEK293T cells

1 grown on 10 cm plates were transiently transfected for 48 h with 8  $\mu$ g plasmid DNA and 25  $\mu$ l  
2 Lipofectamine 2000 (Invitrogen) according to the manufacturer's instructions. One plate was  
3 used for the transfection of each construct in each experiment.

## 5 **HeLa BORCS8 KO generation and genotyping**

6 BORCS8-KO HeLa cells were generated using CRISPR-Cas9 as described.<sup>23</sup> Briefly, the  
7 *BORCS8*-targeting guide RNAs TTCCCGGTTTCGCTCGGCCG and  
8 CTTTAATTACCGGTCCCCC were cloned separately into pSpCas9 (BB)-2A-GFP plasmid  
9 (Addgene, 48138; from Feng Zhang). HeLa cells were co-transfected with the two plasmids, and,  
10 after 48 h, GFP-positive cells were selected on a FACSAria II cell sorter (BD Biosciences).  
11 Single-cell clones were isolated on 96-well plates. After 21 days, genomic DNA was extracted,  
12 and the region around the targeted sequences amplified by PCR with  
13 TTGTCCGCAAAGACTGAGGAG and AGCGATTACTACGCCCG primers. Genotyping of  
14 wild-type (WT) and BORCS8-KO HeLa cells generated 745-bp and 513-bp fragments,  
15 respectively. The resulting deletion of part of the first exon and first intron in *BORCS8* was  
16 confirmed by Sanger sequencing of the amplified region.

## 18 **SDS-PAGE and immunoblotting**

19 Cells were washed twice with ice-cold phosphate-buffered saline (PBS; Corning), scraped from  
20 the plates in 1X Laemmli sample buffer (1xLSB) (Bio-Rad) supplemented with 2.5% v/v 2-  
21 mercaptoethanol (Sigma-Aldrich), heated at 95°C for 5 min, and resolved by SDS-PAGE. Gels  
22 were blotted onto nitrocellulose membrane and blocked with 5% w/v non-fat milk in Tris-  
23 buffered saline, 0.1% v/v Tween 20 (TBS-T) for 20 min. Membranes were sequentially  
24 incubated with primary antibody and secondary HRP-conjugated antibody diluted in TBS-T.  
25 SuperSignal West Dura Reagents (Thermo Fisher) were used for detection of the antibody signal  
26 with a Bio-Rad Chemidoc MP imaging system. Controls for sample loading were either GAPDH  
27 or  $\beta$ -actin.

28

## 1 **Immunoprecipitation**

2 Transfected HEK293T cells were lifted in ice-cold PBS and centrifuged at 500 x g for 5 min.  
3 The pellet was washed twice with ice-cold PBS and lysed in 10 mM Tris-Cl pH 7.5, 150 mM  
4 NaCl, 0.5 mM EDTA, 0.5% v/v Nonidet P40 supplemented with a protease inhibitor cocktail  
5 (Roche). Cell lysates were clarified by centrifugation at 17,000 x g for 10 min and the  
6 supernatant (10% was saved as input) was incubated with anti-HA magnetic agarose beads  
7 (Thermo Fisher) at 4°C for 1 h. After three washes with 10 mM Tris-Cl pH 7.5, 150 mM NaCl,  
8 0.5 mM EDTA, the precipitates were eluted with 1X LSB at 95°C for 5 min. The  
9 immunoprecipitated samples and inputs were analyzed by SDS-PAGE and immunoblotting.

10

## 11 **Immunofluorescence microscopy**

12 Cells were seeded on collagen-coated coverslips in 24-well plates at 40,000 cells per well in  
13 regular culture medium. Cells were then fixed in 4% w/v paraformaldehyde (Electron  
14 Microscopy Sciences) in PBS for 20 min, permeabilized and blocked with 0.1% w/v saponin, 1%  
15 w/v BSA (Gold Bio) in PBS for 20 min, and sequentially incubated with primary and secondary  
16 antibodies diluted in 0.1% w/v saponin, 1% w/v BSA in PBS for 30 min at 37°C. Coverslips  
17 were washed three times in PBS and mounted on glass slides using Fluoromount-G (Electron  
18 Microscopy Sciences) with DAPI. Z-stack cell images were acquired on a Zeiss LSM 780  
19 inverted confocal microscope (Carl Zeiss) using a Plan-Apochromat 63X objective (NA=1.4).  
20 Maximum intensity projections were generated with Zeiss ZEN Black software, and final  
21 composite images were created using ImageJ/Fiji (<https://fiji.sc/>).

22

## 23 **Zebrafish methods**

24 Wild-type (WT) *Danio rerio* (AB/TL strain) were maintained at 28°C at a light/dark cycle of  
25 12/12 h in accordance with standard practices.<sup>24</sup> Embryos were raised at 28.5°C, and collected  
26 and staged as previously described.<sup>25</sup> All experiments were performed in compliance with the  
27 guidelines of the Canadian Council for Animal Care and the local ethics committee of INRS. For

1 immunohistochemical studies, pigment formation was blocked by adding 0.003% phenylthiourea  
2 (PTU) dissolved in egg water at 24 h after fertilization (hpf).

3

#### 4 **Quantification and statistics**

5 Band intensities of BORC subunits in immunoblots from 3-4 independent experiments were  
6 determined using Image Lab (Bio-Rad) and normalized to  $\beta$ -actin or GAPDH. To quantify the  
7 distribution of LAMP1, cells were plated on collagen, imaged, and maximum intensity  
8 projections of z-stack confocal micrographs were subjected to shell analysis<sup>26</sup> (see Fig. 5G).  
9 Briefly, cells exhibiting morphologies where perinuclear clusters of lysosomes were situated too  
10 close to the plasma membrane were excluded from analysis. Cell outlines were traced in Fiji  
11 (<https://imagej.net/software/fiji/>) and the total fluorescence of LAMP1 signal was measured.  
12 Using the “enlarge” function in Fiji, the cell outline was shrunk by 2  $\mu$ m, and LAMP1 signal  
13 intensity re-measured. The intensity of LAMP1 signal within the peripheral 2- $\mu$ m shell was  
14 plotted as percentage of total cellular LAMP1 signal. One-way analysis of variance (ANOVA),  
15 followed by multiple comparisons using the Dunnett’s or Tukey’s test, was used for statistical  
16 analysis of most data sets; the paired Student’s t test was used when comparing two datasets like  
17 in Fig. 5C. All zebrafish experiments were performed on at least three replicates (N), and each  
18 consisted of a sample size (n) of 8-72 fish. All zebrafish data values are given as means  $\pm$  SEM.  
19 Significance for the zebrafish experiments was determined using either Student’s t test or one-  
20 way ANOVA followed by multiple comparisons test. Statistical analyses were done using Prism  
21 version 9 (GraphPad Software).

22

#### 23 **Additional materials and methods**

24 Additional materials and methods are described in the Supplementary material file. These  
25 include materials and methods for work with human cells (culture of human skin fibroblasts,  
26 prediction of BORC complex structure, plasmids, antibodies and chemicals) and zebrafish  
27 (generation of *borcs8* F0 KO zebrafish and rescue experiments, behavioral assays, phalloidin  
28 staining, analysis of NMJ morphology, motor axon visualization, H&E brain staining, and AChE  
29 activity).

# 1 **Results**

2

## 3 **Clinical findings**

4 This study involved three unrelated families (FI, FII and FIII) with five children (FI:1, FI:2,  
5 FII:1, FII:2 and FIII:1) presenting with an early-infantile neurological disorder (Fig. 1A and  
6 Supplementary Fig. 1). Clinical and genetic analyses were conducted as described below and  
7 summarized in Table 1 and Supplementary Tables 1 and 2. Dysmorphology analyses are  
8 summarized in Supplementary Table 3.

9

### 10 **Patient FI:1**

11 Patient FI:1 (Fig. 1A and B and Supplementary Fig. 1) is a 14-year-old European-American  
12 female, the first child born to non-consanguineous parents. She was delivered after induction at  
13 39 weeks of gestation due to maternal hypertension. The fetal movements were described as  
14 normal, with normal ultrasound exams. At birth, she weighed 3.23 kg, and her length was 52.07  
15 cm. She was discharged home after 24 h. She had normal development until 3-4 months of age,  
16 with no subsequent developmental progress, including walking and speech acquisition. At  
17 approximately 1 year of age, she was noted to smile and laugh, but it was unclear if the laughter  
18 was an appropriate response. She developed seizures at 15 months of age, including generalized  
19 tonic seizures and recurrent myoclonic seizures. At 10 years of age, she weighed 36.1 kg with an  
20 occipitofrontal circumference (OFC) of 53 cm. She had a dry scalp and face, hypertelorism,  
21 arched thick eyebrows, up-slanting palpebral fissures, bulbous nasal tip, anteverted nares,  
22 protruding tongue that peels, dry full lips (Fig. 1B and Supplementary Table 3), scoliosis,  
23 abnormal postures of the four limbs predominating in the distal parts, muscle atrophy in legs and  
24 arms, global hypotonia with absent patellar reflexes, and a history of bilateral femur fractures,  
25 kidney stones, cortical visual impairment with optic atrophy, airway clearance issues, and G-tube  
26 dependency. At 14 years of age, she is non-verbal, wheelchair dependent, and needs support for  
27 head control and sitting independently (Fig. 1B and Supplementary Video 1). Previous negative

1 clinical testing includes chromosomal microarray, karyotype, analysis of mitochondrial tRNA,  
2 leukodystrophy panel, hereditary spastic paraplegia panel, and symptom-driven exome.

3 Brain MRI at 1 year of age showed moderate cerebral white matter volume reduction and  
4 delayed myelination associated with ventricular dilatation, thin corpus callosum, mild  
5 enlargement of the cerebral subarachnoid spaces, and very small thalami (Supplementary Fig.  
6 2A-D). The pons and inferior cerebellar vermis were small with associated mega cisterna magna,  
7 while the cerebellar hemispheres volume and cerebellar white matter signal were normal  
8 (Supplementary Fig. 2A-D). A follow-up MRI at 9 years of age showed disease progression with  
9 severe cerebral atrophy, enlargement of the subarachnoid spaces and lack of myelination  
10 progression, additional focal T2/FLAIR signal alterations in the frontal periventricular regions,  
11 further reduction of the thalamic volume, and optic nerve atrophy (Fig. 2). Marked T2  
12 hypointensity and T1 hyperintensity of the globi pallidi were also noted (Supplementary Fig. 3A-  
13 D).

14

## 15 **Patient FI:2**

16 Patient FI:2 (Fig. 1A and B and Supplementary Fig. 1) is an 11-year-old European-American  
17 male, the second child born to the same parents as patient FI:1. He was born at 37 weeks of  
18 gestation following a pregnancy complicated by maternal hypertension and gestational diabetes,  
19 which was monitored. Prenatal ultrasounds were normal. At delivery, he weighed 3.2 kg and was  
20 48.3-cm long. The umbilical cord was reported to be wrapped around his neck and he required  
21 oxygen for 15 min; however, he was discharged home after 3-4 days with no further  
22 complications. He had normal development until 3-4 months of age, with no subsequent  
23 developmental progress, including walking and speech acquisition. He developed intractable  
24 seizures by 1 year of age. At 7 years of age, he weighed 27.2 kg with an OFC of 52.5 cm. A  
25 physical exam found dry skin on scalp and face, hypotonic facies, hypertelorism, arched thick  
26 eyebrows, up-slanting palpebral fissures, very large ears, bulbous nasal tip, anteverted nares,  
27 high palate, thick full lips (Fig. 1B and Supplementary Table 3), bilateral everted ankles,  
28 contractures in knees and some finger joints, muscle atrophy in arms and legs, global hypotonia  
29 and absent patellar reflexes. Additionally, he had airway clearance issues and G-tube  
30 dependency. At 11 years of age, he remains non-verbal, wheelchair dependent, and needs

1 support for head control and sitting independently (Fig. 1B and Supplemental Video 2). Other  
2 genetic testing included chromosomal microarray, karyotype, and an epilepsy sequencing panel,  
3 which showed normal or non-diagnostic results.

4 Brain MRI performed at 7.7 years of age revealed moderate volume reduction and lack of  
5 myelination of the supratentorial white matter with consequent ventricular enlargement and thin  
6 corpus callosum (Fig. 2). Additional focal T2 signal alterations were noted in the frontal and  
7 parietal periventricular regions. Moderate-to-severe cerebral cortical atrophy with enlargement of  
8 the subarachnoid spaces was present. The thalami and pons were small. The cerebellar white  
9 matter signal was normal while the foliar CSF spaces were slightly enlarged (Fig. 2). Finally, a  
10 right optic nerve glioma and left optic nerve atrophy were noted (Supplementary Fig. 3E-G). He  
11 had a resection of the optic nerve glioma at 7.5 years of age.

12

### 13 **Patient FII:1**

14 Patient FII:1 (Fig. 1A and B and Supplementary Fig. 1) is a 13-year-old male, the first child of a  
15 consanguineous Iranian-Arab family. The healthy parents are first cousins. The patient's prenatal  
16 and perinatal history were unremarkable, and he was born at term with his growth parameters all  
17 within normal range (2.75 kg weight, 59 cm length). However, his development was  
18 significantly delayed in all domains. At present, he is non-verbal and has no eye contact with  
19 others, and his level of cognitive impairment is in the range of severe-to-profound  
20 (Supplementary Video 3). Medical examination at the age of 13 years showed postnatal  
21 microcephaly, failure to thrive, no language and hand skills, inability to walk, head nodding  
22 stereotypies, hand rubbing/wringing stereotypies, drooling, tongue thrusting, axial hypotonia,  
23 muscle atrophy and lower limb spasticity (Fig. 1B and Supplementary Video 3). He had a  
24 Babinski sign and brisk tendon reflexes (Supplementary Video 3). His vision was poor, but  
25 hearing was within normal range. Facial dysmorphism included long and narrow face, upswept  
26 anterior hairline, prominent supraorbital ridges, deep-set eyes, thick arched eyebrows, long  
27 eyelashes, long or large ears, high nasal bridge, full nasal tip, low-set columella, bow-shaped  
28 upper lip, flared alae nasi, and tall chin (Fig. 1B, Supplementary Table 3 and Supplementary  
29 Video 3). Additionally, he had long and slender fingers, broad and round distal thumbs, long

1 toes, overriding of hallux and third toe by second toe, deep plantar crease, thin trunk and  
2 extremities (Fig. 1B, Supplementary Table 3 and Supplementary Video 3).

3 Brain MRI at 1 year of age demonstrated moderate white matter volume reduction and  
4 delayed myelination with associated ventricular dilatation especially in the parieto-occipital  
5 regions, thin corpus callosum, mild enlargement of the cerebral subarachnoid spaces, and very  
6 small thalami (Supplementary Fig. 2E-H). The pons and inferior cerebellar vermis were small  
7 with associated mega cisterna magna, while the cerebellar hemispheres volume and cerebellar  
8 white matter signal were normal (Supplementary Fig. 2E-H). Follow-up MRI at 13 years of age  
9 showed disease progression with moderate cerebral and cerebellar atrophy, lack of myelination  
10 progression, further reduction of the thalamic volume, mild T2 hypointensity of the globi pallidi,  
11 and optic nerve atrophy (Fig. 2). Additional focal T2/FLAIR signal alterations were noted in the  
12 frontal and parietal periventricular regions, with an “ears of the lynx” pattern in the frontal lobes  
13 (Supplementary Fig. 3H and I).

14

## 15 **Patient FII:2**

16 Patient FII.2 (Fig. 1A and B and Supplementary Fig. 1) is an 11-year-old female, the second  
17 child of the Iranian-Arab family FII. Her prenatal and perinatal history and metabolic  
18 investigations were unremarkable. She was born at term with normal growth parameters (3 kg  
19 weight, 48 cm length). However, she had global developmental delay with severe-to-profound  
20 intellectual disability and failure to thrive. At present, she cannot speak and has no eye contact  
21 with others. Neurological examination at 11 years of age showed postnatal microcephaly, no  
22 language, no hand skills, inability to walk, hand rubbing/wringing stereotypies, axial hypotonia,  
23 and spasticity and muscle atrophy of the lower limbs (Supplementary Video 4). She has a  
24 Babinski sign and brisk tendon reflexes (Supplementary Video 4). Ophthalmic examination at  
25 the age of 2 years revealed bilateral optic atrophy. Hearing was normal. She has facial  
26 dysmorphic features including bifrontal narrowing, arched eyebrows, synophrys, full nasal tip  
27 and prominent heels (Fig. 1B, Supplementary Table 3 and Supplementary Video 4).

28 Brain MRI performed at 2 years of age revealed mild volume reduction and diffuse T2  
29 hyperintensity of the cerebral white matter in keeping with absent myelination, with associated  
30 ventricular dilatation especially in the parieto-occipital regions, thin corpus callosum, mild

1 enlargement of the cerebral subarachnoid spaces, and very small thalami (Supplemental Fig. 2I-  
2 L). Additional focal T2/FLAIR signal alterations were noted in the frontal and parietal  
3 periventricular regions, with an anterior “ears of the lynx” pattern lobes (Supplementary Fig.  
4 3J,K). The cerebellar volume and white matter signal were normal (Supplementary Fig. 2I-L).  
5 Follow-up brain MRI at 12 years of age showed disease progression with mild cerebral and  
6 moderate cerebellar atrophy, lack of myelination progression, further reduction of the thalamic  
7 volume, mild T2 hypointensity of the globi pallidi, and optic nerves atrophy (Fig. 2). The fronto-  
8 parietal periventricular T2/FLAIR signal alterations were accentuated (Fig. 2).

9

### 10 **Patient FIII:1**

11 Patient FIII.1 (Fig. 1A and B and Supplementary Fig. 1) is a 3-year-old female, the only child of  
12 a consanguineous Egyptian family. Parents are healthy and there is no history of similar  
13 conditions reported in the extended family. The pregnancy history noted weak fetal movement  
14 and maternal preeclampsia, and delivery was by elective Cesarean section. The measurements at  
15 birth were: 3.1 kg weight, 48 cm length, and 33.5 cm OFC. After birth, she was irritable, had  
16 excessive crying, and refused to suckle. At the end of the first day, she was admitted to the NICU  
17 for 8 days, where hyperbilirubinemia and hypocalcemia were recorded. Her developmental  
18 milestones were severely delayed. She did not acquire any motor or cognitive skills and had an  
19 apparently progressive course as she had some visual tracking and social smile at 3 months old.  
20 She suffered from recurrent choking spells followed by chest infections. On examination, she  
21 was lethargic, encephalopathic, not reacting to her surroundings, and had absent speech. Seizures  
22 started at the age of 8 months, were intractable with myoclonic and focal patterns, recurred 4-8  
23 times per day, did not respond to several drug combinations including valproate, levetiracetam,  
24 vigabatrin, topiramate, and clonazepam. The anthropometric measurements at 3 years of age  
25 identified a weight of 13 kg, length of 85 cm and OFC of 45 cm. The patient had a hypotonic  
26 face, a sloping forehead, sparse hair, wide-spaced eyes, an upturned nose, long philtrum,  
27 retruded mandible, and low-set ears (Fig. 1B and Supplementary Table 3). General examination  
28 was unremarkable, and neurological evaluation showed generalized hypotonia (both axial and  
29 limbs) with hyporeflexia. Laboratory tests showed normal karyotype, metabolic screening,  
30 acylcarnitine profile, organic acid in urine, ammonia and lactate in plasma, and auditory

1 brainstem response (ABR). Liver transaminases were elevated (ALT: 113 and AST: 52). EEG  
2 revealed subcortical epileptogenic discharges. Pallor of the optic nerves was observed at fundus  
3 oculi examination. Brain MRI performed at 3 years of age showed severe cerebral and mild  
4 cerebellar atrophy with supratentorial ventricle dilatation, lack of supratentorial white matter  
5 myelination with sparing of the cerebellar white matter, thin corpus callosum, very small  
6 thalami, optic nerve atrophy, and pontine and inferior vermis hypoplasia with mega cisterna  
7 magna (Fig. 2).

8

### 9 **Identification of biallelic variants in *BORCS8***

10 In family FI, quad familial research exome and genome sequencing of DNA from the affected  
11 siblings (FI:1 and FI:2) and their parents identified two variants in *trans* in *BORCS8*: a  
12 maternally inherited frameshift variant [NM\_001145783.2:c.71\_75dup(p.Asn26Trpfs\*51)] and a  
13 paternally inherited missense variant [NM\_001145783.2:c.85T>C(p.Ser29Pro)] (Fig. 1A). The  
14 frameshift variant is not present in ~2,000,000 alleles/chromosomes across multiple large,  
15 aggregated sequence databases (Supplementary Table 2). This variant results in substitution of  
16 Trp for Asn-26 and replacement of the remaining 93 amino acids by 49 extraneous amino acids  
17 (henceforth denoted N26W\*) (Fig. 3A and B). The missense variant, on the other hand, is  
18 present in 35 carriers in the European population. This variant encodes a substitution of Pro for  
19 the highly conserved Ser-29 [Genomic Evolutionary Rate Profiling (GERP) score 4.71 and  
20 Combined Annotation Dependent Depletion (CADD) score 25.6] (Fig. 3A and B and  
21 Supplementary Table 2), and is predicted to be damaging/deleterious and disease-causing by  
22 most *in-silico* tools (Supplementary Table 2).

23 In family FII, research exome sequencing of DNA from the two siblings (FII:1 and  
24 FII:2), confirmed by Sanger sequencing, identified a novel homozygous *BORCS8* missense  
25 variant [(NM\_001145784.2):c.196A>C (p.Thr66Pro)] (Fig. 1A). This variant is within a sizable  
26 region of homozygosity and is absent from all the inspected variant databases. It encodes a  
27 substitution of Pro for the highly conserved Thr-66 (GERP score 4.24 and CADD score 28.4)  
28 (Fig. 3A and B and Supplementary Table 2), and is predicted to be damaging/deleterious and  
29 disease-causing by most *in-silico* tools (Supplementary Table 2).

1 In family FIII, clinical exome sequencing of the proband (FIII-1) identified a novel  
2 homozygous missense variant in *BORCS8* [(NM\_001145784.2):c.124T>C (p.Ser42Pro)]  
3 residing within a large region of homozygosity. This variant was not observed in any variant  
4 frequency databases. It encodes a substitution of Pro for the highly conserved Ser-42 (GERP  
5 score 4.71 and CADD score 28.3) (Fig. 3A and B), and is predicted to be damaging/deleterious  
6 and disease-causing by the majority of employed *in-silico* tools (Supplementary Table 2).

7 In all three families, no additional variants of unknown significance, pathogenic or likely  
8 pathogenic, associated with neurodevelopmental or neurodegenerative disorders were identified.

9 *BORCS8* encodes a protein of 119 amino acids named *BORCS8* or *MEF2BNB*  
10 (<https://www.ncbi.nlm.nih.gov/gene/729991>). *BORCS8* is a subunit of the hetero-octameric  
11 BLOC-one-related complex (*BORC*) (Fig. 3C-E), previously shown to mediate ARL8-dependent  
12 regulation of lysosome motility and positioning.<sup>1</sup> The N26W\* variant removes most of a  
13 predicted long  $\alpha$ -helix (Fig. 3C-E), resulting in a protein with only 25 N-terminal amino acids  
14 from the normal protein, followed by an irrelevant sequence. The substitutions to Pro in the  
15 missense variants likely cause destabilization by disruption of the long  $\alpha$ -helix.

## 17 **Reduced assembly of *BORCS8* variants**

18 To determine the properties of the patients' variants in cells, we obtained cultured skin fibroblast  
19 from patients FI:1 and FI:2, and from their unaffected mother as a control. Cells from families  
20 FII and FIII were not available for analysis. Immunoblot and immunofluorescence microscopy  
21 analyses for *BORCS8* itself in family FI fibroblasts were unsuccessful because several  
22 commercial and house-made antibodies failed to recognize the endogenous protein. As an  
23 alternative, we performed immunoblot analysis of the fibroblasts for *BORCS5* and *BORCS7*, for  
24 which there are suitable antibodies. For this analysis, we also included two additional human  
25 skin fibroblast cultures from a healthy individual (Control 1: 85E0344) and from an SPG50  
26 patient that carries pathogenic mutations in the *AP4M1* and *ATS* genes (Control 2: 87RD39).<sup>18,19</sup>  
27 This analysis revealed no significant differences in the levels of *BORCS5* and *BORCS7* in  
28 fibroblasts from the mother and the unrelated controls, but a significant 45-60% reduction in  
29 *BORCS5* and *BORCS7* levels in the patient's fibroblasts relative to fibroblasts from the mother

1 and the unrelated controls (Fig. 3F and G). These findings indicated that the *BORCS8* N26W\*  
2 and S29P variants resulted in reduced levels of other BORC subunits. Quantitative real-time  
3 reverse-transcription PCR (qRT-PCR) revealed equal levels of *BORCS8*, *BORCS5* and *BORCS7*  
4 mRNAs in fibroblasts from the mother and both patients (Supplementary Fig. 4A and B),  
5 indicating that the variants did not decrease mRNA levels but likely destabilized the  
6 corresponding proteins.

7 To directly analyze the effect of the individual variants on the expression and assembly of  
8 *BORCS8* itself, we next used a heterologous system in which WT and *BORCS8*-mutant proteins  
9 tagged with a C-terminal HA epitope were expressed by transient transfection in HEK293T cells.  
10 Immunoblotting of cell extracts showed that whereas the WT, S29P, T66P and S42P mutants  
11 were expressed at similar levels, the N26W\* mutant was expressed at ~40% levels of the WT  
12 and other mutants (Fig. 4A-D, 10% input lanes). Real-time qRT-PCR showed that the WT,  
13 N26W\* and S29P *BORCS8* mRNAs were expressed at similar levels (Supplementary Fig. 4C).  
14 Incubation with the proteasome inhibitor MG132 did not change the levels of WT and S29P but  
15 increased the levels of N26W\* *BORCS8* (Fig. 4E). These findings are consistent with the lower  
16 levels of the N26W\* mutant protein being at least partly due to proteasomal degradation.

17 Immunoprecipitation from extracts of transfected HEK293T cells expressing *BORCS8*-  
18 HA constructs with antibody to the HA epitope, followed by immunoblotting for endogenous  
19 *BORCS5* and *BORCS7*, showed that co-immunoprecipitation of these subunits was reduced to  
20 30-80% for the S29P, T66P and S42P mutants, and to ~5% for the N26W\* mutant (Fig. 4A-D,  
21 HA IP lanes). The N26W\* co-immunoprecipitation was indistinguishable from that obtained  
22 with the irrelevant KLC1-HA control (Fig. 4A and C), indicating that it was non-specific. From  
23 these experiments, we concluded that, despite being expressed at similar levels than WT  
24 *BORCS8*, the S29P, T66P and S42P mutants were partially impaired in their ability to assemble  
25 with other subunits of BORC. The N26W\* mutant, on the other hand, was not only expressed at  
26 lower levels but was also completely incapable of assembling with other BORC subunits. The  
27 reduced assembly of the *BORCS8* mutant proteins into the complex likely results in partial  
28 degradation of the other subunits, accounting for the reduced levels of both *BORCS5* and  
29 *BORCS7* in the patients' fibroblasts (Fig. 3 F and G). These findings are in line with previous  
30 studies showing a requirement of all subunits for stable assembly of BORC.<sup>9,27</sup>

## 1 **Decreased lysosome-dispersal activity of BORCS8 mutants**

2 To investigate the functional properties of the patients' *BORCS8* variants, we performed rescue  
3 experiments with *BORCS8*-KO HeLa cells (Fig. 5A). Extracts from WT and *BORCS8*-KO HeLa  
4 cells showed reduced amounts of endogenous *BORCS5* and *BORCS7* proteins (Fig. 5B,C), but  
5 not of the corresponding mRNAs (Supplementary Fig. 4D). This confirmed that *BORCS5* and  
6 *BORCS7* were destabilized in the absence of *BORCS8*, and that all the subunits are necessary  
7 for assembly of a stable BORC.<sup>9,27</sup> Cycloheximide chase experiments showed increased turnover  
8 of *BORCS5* and *BORC7* in *BORCS8*-KO relative to WT HeLa cells (Supplementary Fig. 5A  
9 and B), demonstrating that the reduced levels of *BORCS5* and *BORC7* in the absence of  
10 *BORCS8* were due to enhanced degradation. As shown above for HEK293T cells (Fig. 4A-D),  
11 transfection of *BORCS8*-KO cells with plasmids encoding HA-tagged WT and mutant *BORCS8*  
12 constructs showed that the WT, S29P, T66P and S42P proteins were expressed at similar levels,  
13 whereas the N26W\* protein was expressed at lower levels (Fig. 5D).

14 Next, we examined the effect of expressing WT and mutant *BORCS8* proteins on the  
15 distribution of lysosomes labeled for the endogenous lysosomal membrane protein LAMP1 in  
16 *BORCS8*-KO HeLa cells. In agreement with previous findings,<sup>1,8</sup> *BORCS8* KO caused  
17 clustering of lysosomes in the juxtannuclear area of the cells and their depletion from the  
18 peripheral cytoplasm (Fig. 5E,G and H). Expression of WT *BORCS8* restored the normal  
19 distribution of lysosomes (Fig. 5F-H). In contrast, expression of the *BORCS8* mutants resulted in  
20 partial (S29P, T66P) or no rescue (N26W\*, S42P) (Fig. 5F-H). These observations demonstrated  
21 that the patients' *BORCS8* variants have reduced ability to distribute lysosomes toward the  
22 peripheral cytoplasm.

23 *BORCS8* KO has also been shown to increase the levels of the autophagy protein LC3B,  
24 due to inhibition of lysosome-autophagosome fusion<sup>23</sup> (Supplementary Fig. 6A and C). We  
25 observed that re-expression of WT, S29P or T66P *BORCS8* decreased the number of LC3B  
26 puncta in *BORCS8*-KO HeLa cells, whereas re-expression of N26W\* and S42P *BORCS8* did  
27 not (Supplementary Fig. 6B and C). From these experiments, we concluded that at least some of  
28 the *BORCS8* mutants compromise the ability of lysosomes to fuse with autophagosomes.  
29 Differences in the activity of the S29P in T66P mutants in lysosome dispersal (Fig. 5) and LC3B  
30 reduction (Supplementary Fig. 6) may be due to the different sensitivity of each assay.

## 1 **Neurodevelopmental defects in *borcs8*-KO zebrafish**

2 A role for BORCS8 in neurodevelopment had not been demonstrated prior to this work. To  
3 assess this role in a vertebrate model, we examined the effect of knocking out *borcs8* in  
4 zebrafish. The zebrafish genome encodes a single *borcs8* ortholog that shares 67% nucleotide  
5 and 76% amino-acid identity with human *BORCS8/BORCS8*. We generated a *borcs8* F0 KO  
6 model using CRISPR-Cas9.<sup>28</sup> To this end, we used three sets of Cas9-gRNA ribonucleoproteins  
7 (RNPs) to target *borcs8* (Supplementary Fig. 7A), thereby generating a biallelic zygotic KO  
8 directly in the injected embryos (F0 generation). Using a high-resolution melting assay,<sup>29</sup> we  
9 found that RNPs were very efficient in creating indels in injected embryos (Supplementary Fig.  
10 7B). Sequencing of injected embryos revealed mutations at the targeted loci, with a high  
11 percentage of indels leading to premature stop codons (Supplementary Fig. 7C and D).

12 We found that at 3 days postfertilization (3 dpf) *borcs8* F0 KO larvae exhibited a smaller  
13 body size (intermediate phenotype), with some of the larvae exhibiting a slight curvature of the  
14 body axis (strong phenotype) (Fig. 6A-C), as compared to WT controls. Injections of Cas9  
15 protein alone as a control showed no morphological defects compared to WT larvae (Fig. 6A-C).  
16 Additionally, the *borcs8* F0 KO 3 dpf fish displayed a smaller head (Fig. 6D) and eye size (Fig.  
17 6E) compared to WT controls and Cas9-expressing control fish. These morphological defects  
18 persisted at 5 dpf (Supplementary Fig. 8A-C). We further examined these fish at the histological  
19 level on transverse brain sections at 3 dpf (Supplementary Fig. 7E) and 5 dpf (Fig. 6F and G).  
20 Hematoxylin and eosin (H&E) staining revealed significant structural differences and smaller  
21 brain size in 5 dpf brains from *borcs8* F0 KO relative to WT larvae (Fig. 6F and G). These  
22 differences were not evident at 3 dpf (Supplementary Fig. 7E), suggesting that structural brain  
23 abnormalities in *borcs8* F0 KO fish are progressive.

24 Normalization of head and eye areas to body length at 3 dpf revealed no differences in  
25 both ratios in *borcs8* F0 KO larvae compared to WT controls (Supplementary Fig. 8D,E).  
26 Similarly, no differences were observed in normalized head and brain areas to body length at 5  
27 dpf, but the eye area:body length ratio was significantly reduced in *borcs8* F0 KO larvae  
28 (Supplementary Fig. 8F-H). Altogether, these data suggest a global developmental delay in  
29 *borcs8*-KO zebrafish, consistent with clinical findings in the children bearing mutations in  
30 *BORCS8*. To test the specificity of the morphological phenotypes in *borcs8* KO fish, mRNA

1 encoding human *BORCS8* (Rescue) was injected along with RNPs, resulting in significant rescue  
2 of the head, eye and brain areas, and the body length defects (Fig. 6C-E and G).

3         Given the clinical findings of hypotonia and limb spasticity in patients bearing *BORCS8*  
4 mutations, we assessed neuromuscular morphology and locomotion in *borcs8* F0 KO larvae. The  
5 areas of dorsal and ventral myotomes of 3-dpf *borcs8* F0 KO larvae were significantly reduced  
6 (Fig. 6H and I). Additionally, the myosepta of *borcs8* F0 KO larvae were markedly narrower  
7 than in control larvae (Fig. 6J). Along with these muscle phenotypes, we found that the motor  
8 neurons, which innervate the myotomes, have shorter and less branched axons (Fig. 7A and B).  
9 The motor axonal defects in *borcs8* F0 KO zebrafish were significantly rescued upon expression  
10 of the human *BORCS8* mRNA (Fig. 7B). We next examined neuromuscular junction (NMJ)  
11 integrity by performing double immunohistochemistry using specific presynaptic (SV2) and  
12 postsynaptic ( $\alpha$ -bungarotoxin) markers. We observed a drastic alteration in NMJ morphology  
13 with reduced presynaptic and postsynaptic staining in 3 dpf (Fig. 7C) and 5 dpf (Supplementary  
14 Fig. 9A) *borcs8* F0 KO larvae compared to WT controls, and a reduction in the number of  
15 colocalizing presynaptic and postsynaptic puncta in *borcs8* F0 KO larvae (Fig. 7D;  
16 Supplementary Fig. 9B). This decrease in synaptic puncta at NMJs in *borcs8* F0 KO fish was  
17 accompanied by a significant reduction in acetylcholinesterase (AChE) activity (Supplementary  
18 Fig. 9C). Further analysis revealed no change in colocalization of presynaptic and postsynaptic  
19 puncta in *borcs8* F0 KO at early embryonic developmental stages (2 dpf; Supplementary Fig. 9D  
20 and E). However, 2 dpf *borcs8* F0 KO larvae displayed impaired movement after touch (i.e.,  
21 touch-evoked escape response) (Fig. 7E), and 5 dpf larvae decreased locomotor activity (i.e., free  
22 swimming), as compared to controls (Fig. 7F). No significant changes in free-swimming activity  
23 between *borcs8* F0 KO fish and WT controls were observed at early developmental stages (2 and  
24 3 dpf; Supplementary Fig. 9F and G). These findings thus indicated that *borcs8* F0 KO larvae  
25 had neuromuscular defects with a strong impact on motor function. Moreover, our data suggest  
26 that the defects in NMJ morphology and locomotor activity were progressive with larval age,  
27 consistent with the neurodegenerative findings in patients bearing *BORCS8* mutations.

28         Taken together, the zebrafish experiments confirmed that *borcs8* is critical for the  
29 development and function of the CNS.

30

## 1 Discussion

2 Here we report five children from three unrelated families with biallelic variants in *BORCS8*.  
3 These children present with global developmental delay, severe-to-profound intellectual  
4 disability, facial dysmorphism, variable neurological features including seizures, spasticity,  
5 stereotypies, cortical visual impairment, and consistent neuroradiological findings. The latter  
6 include cerebral and cerebellar atrophy, white matter hypomyelination, hypoplasia of the pons,  
7 thin corpus callosum, small thalami, and optic atrophy. In addition, focal white matter signal  
8 alterations with an “ears of the lynx” sign were noted in two subjects, and T2 hypointensity of  
9 globus pallidi was evident in another patient. Many of these features were apparent on initial  
10 MRI scans at the age of 1-3 years, with the rest becoming noticeable on follow-up scans several  
11 years later. In line with these findings, biallelic KO of *borcs8* in zebrafish leads to  
12 neurodevelopmental defects and loss of motility. These findings demonstrate that BORCS8 is  
13 critical for the development and function of the CNS in vertebrates.

14 The neuroimaging findings in the BORCS8-deficient patients overlap with those of other  
15 congenital neurological disorders and, in combination, could help with the diagnosis of this  
16 condition. Hypomyelination is a key feature of a large number of disorders, many of which  
17 present with developmental disability (DD), intellectual disability (ID), and/or facial  
18 dysmorphism.<sup>30</sup> Among these disorders are Pelizaeus-Merzbacher disease, Pelizaeus-  
19 Merzbacher-like disease, 4H syndrome, Salla disease, hypomyelination and congenital cataract,  
20 and 18q deletion syndrome.<sup>30</sup> Of note, hypomyelination associated with neurodegenerative  
21 features is also common in infantile-onset lysosomal neuronal storage disorders, such as infantile  
22 GM1 and GM2 gangliosidosis, fucosidosis and neuronal ceroid lipofuscinoses, in which  
23 myelination is perturbed due to axonal dysfunction and degeneration starting before myelination  
24 has reached completion.<sup>31</sup>

25 Small thalami are a feature of postnatal progressive microcephaly with seizures and brain  
26 atrophy caused by biallelic variants in *MED17*,<sup>32</sup> and neurodevelopmental disorder with seizures  
27 and brain atrophy caused by biallelic variants in *EXOC7*.<sup>33</sup> Thin corpus callosum with “ear of the  
28 lynx sign” can be seen in hereditary spastic paraplegia due to biallelic *SPG11* and *SPG15*  
29 variants, both characterized by lysosomal dysfunction.<sup>34</sup> Neurodevelopmental impairments with  
30 T2 hypointensity of the globus pallidi in children suggests connections to a form of

1 neurodegeneration with brain iron accumulation (NBIA).<sup>35,36</sup> NBIA is now a fairly large group of  
2 disorders, but childhood-onset NBIA with MRI features overlapping with those seen in children  
3 with biallelic *BORCS8* variants (i.e., globus pallidi T2 hypointensity plus white matter changes)  
4 include infantile neuroaxonal dystrophy (NBIA2A), fatty acid hydroxylase-associate  
5 neurodegeneration (FAHN; also called hereditary spastic paraplegia type 35), Kufor-Rakeb  
6 syndrome, and Woodhouse-Sakati syndrome.<sup>35, 36</sup> However, when these MRI features are seen  
7 in association with progressive cerebral and cerebellar atrophy, optic atrophy and hypoplasia of  
8 the pons in a child with DD/ID, abnormal neurology and facial dysmorphism, *BORCS8*-related  
9 disorder should be considered a likely diagnosis.

10 The clinical features of the patients with *BORCS8* variants described here are also like  
11 those of a previously reported patient with a homozygous splice variant of *BORCS5* (c203-  
12 1G>T).<sup>17</sup> The exact nature of the transcript and the activity of the *BORCS5* variant protein were  
13 not assessed in the previous study. Nevertheless, the similarities in clinical presentation suggest  
14 that the *BORCS5* variant protein may likewise be defective in expression, assembly and/or  
15 function. Together, these findings begin to define a “BORC-deficiency syndrome” caused by  
16 variants in any of the subunits of this complex, in the same way that an “AP-4 deficiency  
17 syndrome” (a form of hereditary spastic paraplegia) is caused by variants in subunits of the AP-4  
18 complex.<sup>37,38</sup>

19 The *BORCS8* S29P, T66P and S42P substitutions are all predicted to be deleterious by  
20 bioinformatics tools. Their deleterious effects are likely due to destabilization of the long  $\alpha$ -helix  
21 by the irregular geometry of the substitute Pro. The N26W\* variant, on the other hand, results in  
22 deletion of most of the long  $\alpha$ -helix and its partial replacement by an irrelevant sequence. This  
23 latter variant has little of the normal *BORCS8* and is thus also expected to be deleterious. Indeed,  
24 analyses using a heterologous cell system show that all *BORCS8* variants are functionally  
25 defective (see Supplementary Table 4). In transfected HEK293T and HeLa cells, the S29P, T66P  
26 and S42P proteins are expressed at normal levels but display reduced assembly with *BORCS5*  
27 and *BORCS7*. Furthermore, the N26W\* protein is expressed at very low levels because of  
28 proteasomal degradation and does not assemble at all with *BORCS5* and *BORCS7*. KO or  
29 mutations in BORC subunit genes were previously shown to cause destabilization and  
30 degradation of other subunits of the complex.<sup>1,9,11,27</sup> This phenomenon may account for the

1 reduced levels of BORCS5 and BORCS7 in skin fibroblasts of the family FI affected siblings  
2 relative to those of the mother.

3 The variant BORCS8 proteins displayed not only expression and/or assembly defects but  
4 also decreased ability to rescue lysosome dispersal in BORCS8-KO cells. BORC is part of an  
5 adaptor system that couples lysosomes to kinesin-1 and -3 motors for anterograde transport along  
6 microtubule tracks.<sup>1,8</sup> Accordingly, we find that KO of BORCS8 impairs the distribution of  
7 lysosomes toward the peripheral cytoplasm, causing their clustering in the juxtannuclear area of  
8 the cell. Whereas re-expression of WT BORCS8 restored the normal distribution of lysosomes,  
9 all the variants displayed reduced activity in this assay. We were unable to assess the distribution  
10 of lysosomes in fibroblasts from the family F1 siblings vs. their mother because the spindly  
11 shape of the fibroblasts and proximity of lysosomes to the nucleus precluded accurate  
12 quantification of lysosome distribution. Taken together, the above findings demonstrated that the  
13 BORCS8 variants analyzed in this study are likely pathogenic.

14 The severity of phenotypic defects in mice and humans with mutations in BORC-subunit  
15 genes emphasizes the critical importance of lysosome distribution for the maintenance of cellular  
16 homeostasis. This importance derives from the need to distribute not only the degradative  
17 activity of lysosomes, but also their non-degradative roles in signaling, adhesion, and plasma  
18 membrane repair to all regions of the cell.<sup>1,39,40</sup> This ability is even more critical in neurons,  
19 where lysosomes are required for maintenance of axonal health. In our functional assay, we  
20 focused on the function of BORC in promoting anterograde lysosome transport. However,  
21 BORC also mediates ARL8-dependent recruitment of RUFY3, a regulator of lysosome coupling  
22 to the retrograde microtubule motor dynein-dynactin,<sup>40,41</sup> and the HOPS complex, a regulator of  
23 endolysosomal/autophagosomal tethering and fusion.<sup>23,42,43</sup> Indeed, BORCS-KO HeLa cells  
24 exhibited accumulation of the autophagy protein LC3B, which was reversed by re-expression of  
25 WT but not N26W\* or S42P BORCS8. It is thus likely that BORCS8-deficient patients also have  
26 endolysosomal/ autophagosomal fusion defects that contribute to the pathogenesis of the disease.

27 Loss-of-function of *borcs8* in zebrafish resulted in neurodevelopmental defects including  
28 reduced muscle size, motor axon defects, NMJ anomalies and impaired motility, further  
29 supporting a role for *borcs8* in the development and function of the CNS. Some of these defects  
30 were progressive, consistent with the presentation of the disease in humans. These findings are

1 consistent with those in previous studies of BORCS5 and BORCS7 mutant mice, which  
2 displayed a number of neurodevelopmental abnormalities.<sup>9,11</sup> For instance, BORCS7  
3 Q87X/Q87X-mutant mice exhibited motor axonal atrophy and impaired motor function.<sup>11</sup> One  
4 difference with the *borcs8* F0 KO zebrafish is that BORCS5-KO mouse embryos did not display  
5 defects in the diaphragm NMJs, although the innervating phrenic nerve was severely dystrophic.<sup>9</sup>  
6 This differential effect on NMJs could be due to differences in species, developmental stage,  
7 specific NMJs, or BORC subunits mutated. It is noteworthy that BORCS5-KO and BORCS7-KO  
8 mice die neonatally.<sup>9,11</sup> It is thus likely that BORCS8 KO would also be lethal in mice and  
9 humans, and that the partial activity of some of the variants keeps the patients alive, albeit with  
10 severe CNS problems.

11

12 In summary, our results identify *BORCS8* as a novel neurogenetic disease gene, and  
13 BORC-dependent lysosome dynamics as a critical process in human CNS development and  
14 function.

15

## 16 **Data availability**

17 The data that support the findings of this study are available from the corresponding author, upon  
18 reasonable request.

19

## 20 **Acknowledgements**

21 We thank the patients and their parents for their participation in this study. We also thank  
22 Carsten Bönnemann (NINDS, NIH) and Christopher Grunseich (NINDS, NIH) for helpful  
23 discussions. This work utilized the computational resources of the NIH HPC Biowulf cluster  
24 (<http://hpc.nih.gov>).

25

26

27

## 1 **Funding**

2 The study was funded by the generous gifts to Children's Mercy Research Institute and Genomic  
3 Answers for Kids program at Children's Mercy Kansas City, the Intramural Program of the  
4 *Eunice Kennedy Shriver* National Institute of Child Health and Human Development (NICHD)  
5 (project ZIA HD001607 to J.S.B.), The Wellcome Trust, The MRC, The MSA Trust, The  
6 National Institute for Health Research University College London Hospitals Biomedical  
7 Research Centre, The Michael J Fox Foundation (MJFF), BBSRC, The Fidelity Trust, Rosetrees  
8 Trust, Ataxia UK, Brain Research UK, Sparks GOSH Charity, Alzheimer's Research UK  
9 (ARUK) and CureDRPLA (to RM), and the Canadian Institutes for Health Research (CIHR,  
10 OGB-177940 to S.A.P.).

11

## 12 **Competing interests**

13 The authors report no competing interests.

14

## 15 **Supplementary material**

16 Supplementary material is available at *Brain* online.

17

## 18 **References**

- 19 1. Pu J, Schindler C, Jia R, Jarnik M, Backlund P, Bonifacino JS. BORC, a multisubunit  
20 complex that regulates lysosome positioning. *Dev Cell*. 2015;33:176-188.
- 21 2. Filipek PA, de Araujo MEG, Vogel GF et al. LAMTOR/Ragulator is a negative regulator  
22 of Arl8b- and BORC-dependent late endosomal positioning. *J Cell Biol*. 2017;216:4199-  
23 4215.
- 24 3. Pu J, Keren-Kaplan T, Bonifacino JS. A Ragulator-BORC interaction controls lysosome  
25 positioning in response to amino acid availability. *J Cell Biol*. 2017;216:4183-4197.

- 1 4. Schweitzer LD, Comb WC, Bar-Peled L, Sabatini DM. Disruption of the Rag-Ragulator  
2 complex by c17orf59 inhibits mTORC1. *Cell Rep.* 2015;12:1445-1455.
- 3 5. Hofmann I, Munro S. An N-terminally acetylated Arf-like GTPase is localised to  
4 lysosomes and affects their motility. *J Cell Sci.* 2006;119:1494-1503.
- 5 6. Rosa-Ferreira C, Munro S. Arl8 and SKIP act together to link lysosomes to kinesin-1. *Dev*  
6 *Cell.* 2011;21:1171-1178.
- 7 7. Niwa S, Lipton DM, Morikawa M et al. Autoinhibition of a neuronal kinesin UNC-  
8 104/KIF1A regulates the size and density of synapses. *Cell Rep.* 2016;16:2129-2141.
- 9 8. Guardia CM, Farías GG, Jia R, Pu J, Bonifacino JS. BORC functions upstream of kinesins  
10 1 and 3 to coordinate regional movement of lysosomes along different microtubule Tracks.  
11 *Cell Rep.* 2016;17:1950-1961.
- 12 9. De Pace R, Britt DJ, Mercurio J et al. Synaptic vesicle precursors and lysosomes are  
13 transported by different mechanisms in the axon of mammalian neurons. *Cell Rep.*  
14 2020;31:107775.
- 15 10. Farías GG, Guardia CM, De Pace R, Britt DJ, Bonifacino JS. BORC/kinesin-1 ensemble  
16 drives polarized transport of lysosomes into the axon. *Proc Natl Acad Sci U S A.*  
17 2017;114:E2955-E2964.
- 18 11. Snouwaert JN, Church RJ, Jania L et al. A mutation in the Borcs7 subunit of the lysosome  
19 regulatory BORC complex results in motor deficits and dystrophic axonopathy in mice.  
20 *Cell Rep.* 2018;24:1254-1265.
- 21 12. Schiefermeier N, Scheffler JM, de Araujo ME et al. The late endosomal p14-MP1  
22 (LAMTOR2/3) complex regulates focal adhesion dynamics during cell migration. *J Cell*  
23 *Biol.* 2014;205:525-540.
- 24 13. Dykes SS, Gray AL, Coleman DT et al. The Arf-like GTPase Arl8b is essential for three-  
25 dimensional invasive growth of prostate cancer in vitro and xenograft formation and  
26 growth in vivo. *Oncotarget.* 2016;7:31037-31052.

- 1 14. Michelet X, Tuli A, Gan H et al. Lysosome-mediated plasma membrane repair is  
2 dependent on the small GTPase Arl8b and determines cell death type in Mycobacterium  
3 tuberculosis infection. *J Immunol.* 2018;200:3160-3169.
- 4 15. Jia R, Bonifacino JS. Lysosome positioning influences mTORC2 and AKT signaling. *Mol*  
5 *Cell.* 2019;75:26-38.e3.
- 6 16. Korolchuk VI, Saiki S, Lichtenberg M et al. Lysosomal positioning coordinates cellular  
7 nutrient responses. *Nat Cell Biol.* 2011;13:453-460.
- 8 17. Charng WL, Karaca E, Coban Akdemir Z et al. Exome sequencing in mostly  
9 consanguineous Arab families with neurologic disease provides a high potential molecular  
10 diagnosis rate. *BMC Med Genomics.* 2016;9:42.
- 11 18. Verkerk AJ, Schot R, Dumeé B et al. Mutation in the AP4M1 gene provides a model for  
12 neuroaxonal injury in cerebral palsy. *Am J Hum Genet.* 2009;85:40-52.
- 13 19. De Pace R, Skirzewski M, Damme M et al. Altered distribution of ATG9A and  
14 accumulation of axonal aggregates in neurons from a mouse model of AP-4 deficiency  
15 syndrome. *PLoS Genet.* 2018;14:e1007363.
- 16 20. Bertoli-Avella AM, Kandaswamy KK, Khan S et al. Combining exome/genome  
17 sequencing with data repository analysis reveals novel gene-disease associations for a wide  
18 range of genetic disorders. *Genet Med.* 2021;23:1551-1568.
- 19 21. Cohen ASA, Farrow EG, Abdelmoity AT et al. Genomic answers for children: Dynamic  
20 analyses of >1000 pediatric rare disease genomes. *Genet Med.* 2022;24:1336-1348.
- 21 22. Dafsari HS, Pemberton JG, Ferrer EA et al. PI4K2A deficiency causes innate error in  
22 intracellular trafficking with developmental and epileptic-dyskinetic encephalopathy. *Ann*  
23 *Clin Transl Neurol.* 2022;9:1345-1358.
- 24 23. Jia R, Guardia CM, Pu J, Chen Y, Bonifacino JS. BORC coordinates encounter and fusion  
25 of lysosomes with autophagosomes. *Autophagy.* 2017;13:1648-1663.
- 26 24. Westerfield M. The zebrafish book: a guide for the laboratory use of zebrafish. [http://zfin](http://zfin.org/zf_info/zfbook/zfbk.html)  
27 [org/zf\\_info/zfbook/zfbk.html](http://zfin.org/zf_info/zfbook/zfbk.html). 2000

- 1 25. Kimmel CB, Ballard WW, Kimmel SR, Ullmann B, Schilling TF. Stages of embryonic  
2 development of the zebrafish. *Dev Dyn.* 1995;203:253-310.
- 3 26. Williamson CD, Guardia CM, De Pace R, Bonifacino JS, Saric A. Measurement of  
4 lysosome positioning by shell analysis and line scan. *Methods Mol Biol.* 2022;2473:285-  
5 306.
- 6 27. Yordanov TE, Hipolito VEB, Liebscher G et al. Biogenesis of lysosome-related organelles  
7 complex-1 (BORC) regulates late endosomal/lysosomal size through PIKfyve-dependent  
8 phosphatidylinositol-3,5-bisphosphate. *Traffic.* 2019;20:674-696.
- 9 28. Kroll F, Powell GT, Ghosh M et al. A simple and effective F0 knockout method for rapid  
10 screening of behaviour and other complex phenotypes. *Elife.* 2021;10:e59683.
- 11 29. Samarut É, Lissouba A, Drapeau P. A simplified method for identifying early CRISPR-  
12 induced indels in zebrafish embryos using High Resolution Melting analysis. *BMC*  
13 *Genomics.* 2016;17:547.
- 14 30. Steenweg ME, Vanderver A, Blaser S et al. Magnetic resonance imaging pattern  
15 recognition in hypomyelinating disorders. *Brain.* 2010;133:2971-2982.
- 16 31. van der Knaap MS, Bugiani M. Leukodystrophies: a proposed classification system based  
17 on pathological changes and pathogenetic mechanisms. *Acta Neuropathol.* 2017;134:351-  
18 382.
- 19 32. Kaufmann R, Straussberg R, Mandel H et al. Infantile cerebral and cerebellar atrophy is  
20 associated with a mutation in the MED17 subunit of the transcription preinitiation mediator  
21 complex. *Am J Hum Genet.* 2010;87:667-670.
- 22 33. Coulter ME, Musaev D, DeGennaro EM et al. Regulation of human cerebral cortical  
23 development by EXOC7 and EXOC8, components of the exocyst complex, and roles in  
24 neural progenitor cell proliferation and survival. *Genet Med.* 2020;22:1040-1050.
- 25 34. Edmison D, Wang L, Gowrishankar S. Lysosome function and dysfunction in hereditary  
26 spastic paraplegias. *Brain Sci.* 2021;11:152.
- 27 35. Lee JH, Yun JY, Gregory A, Hogarth P, Hayflick SJ. Brain MRI Pattern Recognition in  
28 Neurodegeneration With Brain Iron Accumulation. *Front Neurol.* 2020;11:1024.

- 1 36. Lehericy S, Roze E, Goizet C, Mochel F. MRI of neurodegeneration with brain iron  
2 accumulation. *Curr Opin Neurol.* 2020;33:462-473.
- 3 37. Ebrahimi-Fakhari D, Teinert J, Behne R et al. Defining the clinical, molecular and imaging  
4 spectrum of adaptor protein complex 4-associated hereditary spastic paraplegia. *Brain.*  
5 2020;143:2929-2944.
- 6 38. Mattera R, De Pace R, Bonifacino JS. The role of AP-4 in cargo export from the trans-  
7 Golgi network and hereditary spastic paraplegia. *Biochem Soc Trans.* 2020;48:1877-1888.
- 8 39. Ballabio A, Bonifacino JS. Lysosomes as dynamic regulators of cell and organismal  
9 homeostasis. *Nat Rev Mol Cell Biol.* 2020;21:101-118.
- 10 40. Kumar G, Chawla P, Dhiman N et al. RUFY3 links Arl8b and JIP4-Dynein complex to  
11 regulate lysosome size and positioning. *Nat Commun.* 2022;13:1540.
- 12 41. Keren-Kaplan T, Sarić A, Ghosh S et al. RUFY3 and RUFY4 are ARL8 effectors that  
13 promote coupling of endolysosomes to dynein-dynactin. *Nat Commun.* 2022;13:1506.
- 14 42. Garg S, Sharma M, Ung C et al. Lysosomal trafficking, antigen presentation, and microbial  
15 killing are controlled by the Arf-like GTPase Arl8b. *Immunity.* 2011;35:182-193.
- 16 43. Khatter D, Sindhvani A, Sharma M. Arf-like GTPase Arl8: Moving from the periphery to  
17 the center of lysosomal biology. *Cell Logist.* 2015;5:e1086501.
- 18 44. Berezin C, Glaser F, Rosenberg J et al. ConSeq: the identification of functionally and  
19 structurally important residues in protein sequences. *Bioinformatics.* 2004;20:1322-1324.
- 20 45. Lord SJ, Velle KB, Mullins RD, Fritz-Laylin LK. SuperPlots: Communicating  
21 reproducibility and variability in cell biology. *J Cell Biol.* 2020;219:e202001064.
- 22

## 1 **Figure legends**

2

3 **Figure 1 Family pedigrees and photographs of the patients.** (A) Family pedigrees and  
 4 genotypes. *BORCS8* variants are indicated in blue, with Dup corresponding to the c.71-  
 5 75dupTGGCC (p.Asn26Trpfs\*51) variant, and T/C and A/C to the T>C and A>C single-base  
 6 substitution variants, respectively. (B) Photographs of the patients at the indicated ages.

7

8 **Figure 2 Neuroimaging findings.** Brain MRI studies of a control subject performed at 9 years  
 9 of age for comparison, and of the patients performed at 9 years (FI:1), 7.7 years (FI:2), 13 years  
 10 (FII:1), 12 years (FII:2) and 3 years of age (FIII:1). In the patients, sagittal T1- or T2-weighted  
 11 (left), axial T2-weighted (center) and coronal T1 or T2-weighted images (right) reveal mild-to-  
 12 severe cerebral atrophy with reduced white matter volume and enlarged subarachnoid spaces in  
 13 all cases. There is diffuse T2 hyperintensity of the cerebral white matter in all subjects, with  
 14 relative sparing of the internal capsules and subcortical U-fibers in patients FII:1 and FII:2, in  
 15 keeping with hypomyelination. Focal signal alterations are associated at the level of the fronto-  
 16 parietal white matter. The corpus callosum is thin in all patients (thick arrows). The thalami are  
 17 very small and slightly T2 hypointense in all cases (asterisks). The globi pallidi are small and  
 18 darker on T2 weighted images in patients FI:1, FII:1 and FII:2 (full arrowheads). There is mild  
 19 pontine hypoplasia (thin arrows) and marked optic nerve and chiasm atrophy (thin dashed  
 20 arrows) in all subjects. Mild-to-moderate cerebellar atrophy with prevalent enlargement of the  
 21 hemispheric subarachnoid spaces is present in all subjects (empty arrows), while involvement of  
 22 the superior vermis is visible only in patients FII:1, FII:2 and FIII:1 (empty arrowheads).

23

24 **Figure 3 Characteristics of WT and variant *BORCS8* alleles.** (A) Amino-acid sequence of  
 25 WT *BORCS8* indicating the positions of the variants. (B) Amino-acid conservation of *BORCS8*  
 26 from different species calculated on the ConSeq server (<http://conseq.tau.ac.il/>)<sup>44</sup> using default  
 27 search values. (C) Structure of *BORCS8* extracted from the whole BORC complex predicted by  
 28 AlphaFold Multimer. (D) Structure of the BORC complex predicted by AlphaFold Multimer.  
 29 BORC subunits are shown in different colors. (E) Close-up view of the positions of the variants

1 (highlighted in gray). **(F)** Skin fibroblast cultures from two unrelated controls [a healthy  
2 individual (control 1, 85E0344) and an SPG50 patient (control 2, 87RD39),<sup>18, 19</sup> the unaffected  
3 FI family mother and her affected children were analyzed by SDS-PAGE and immunoblotting  
4 for the endogenous BORCS5 and BORCS7 subunits of BORC.  $\beta$ -actin was used as loading  
5 control. The positions of molecular mass markers (in kDa) are indicated on the left. **(G)**  
6 Quantification of endogenous BORCS5 and BORCS7 levels from at least four independent  
7 experiments such as that shown in panel **F**. Values are the mean  $\pm$  SD from the number of data  
8 points shown on the figure. Statistical significance was calculated by one-way ANOVA followed  
9 by multiple comparisons using Dunnett's test. \*\*\*\* $p < 0.0001$ .

10

11 **Figure 4 BORCS8 patient variants reduce the levels and/or assembly of BORC subunits.**

12 **(A,B)** HEK293T cells were transfected with plasmids encoding the indicated HA-tagged  
13 constructs and subjected to immunoprecipitation with antibody to the HA epitope. Cell extracts  
14 (10%) and immunoprecipitates (HA IP) were analyzed by SDS-PAGE and immunoblotting (IB)  
15 for the HA epitope, endogenous BORCS5 and BORCS7, GAPDH (control) or  $\beta$ -actin (control).  
16 KLC1-HA was used as a non-specific immunoprecipitation control. The positions of molecular  
17 mass markers (in kDa) are indicated on the left. Arrows indicate the positions of the specific  
18 proteins. **(C,D)** Quantification from three independent experiments such as those shown in  
19 panels **A** and **B**. Values are the mean  $\pm$  SD. Statistical significance was calculated by one-way  
20 ANOVA followed by multiple comparisons using Dunnett's test. \* $p < 0.05$ ; \*\* $p < 0.01$ ;  
21 \*\*\*\* $p < 0.0001$ . **(E)** HEK293T cells transfected with HA-tagged BORCS8 constructs were treated  
22 with 40  $\mu$ M of the proteasomal inhibitor MG132 for the indicated times, lysed and  
23 immunoblotted for the HA epitope and GAPDH (loading control). The positions of molecular  
24 mass markers (in kDa) are indicated on the left.

25

26 **Figure 5 BORCS8 patient variants impair the lysosome-dispersal function of BORC. (A)**

27 Agarose gel electrophoresis and GelRed® staining of genomic *BORCS8* PCR products yields  
28 745-bp fragment for WT and 513-bp fragment for BORCS8-KO HeLa cells. **(B)** SDS-PAGE and  
29 immunoblot analysis of WT and BORCS8-KO HeLa cells using antibodies to endogenous  
30 BORCS5 and BORCS7.  $\beta$ -actin was used as a control. The positions of molecular mass markers

1 (in kDa) are indicated on the left. **(C)** Quantification of BORCS5 and BORCS7 levels from three  
 2 independent experiments such as that shown in panel **B**. Values are the mean  $\pm$  SD. Statistical  
 3 significance was calculated by Student's t test. \* $p < 0.05$ ; \*\*\* $p < 0.001$ . **(D)** BORCS8-KO HeLa  
 4 cells were transiently transfected with the indicated HA-tagged BORCS8 constructs, and cell  
 5 extracts were immunoblotted (IB) for the HA epitope and GAPDH (loading control). The  
 6 positions of molecular mass markers (in kDa) are indicated on the left. The positions of specific  
 7 proteins are indicated by arrows. **(E)** WT and BORCS8-KO HeLa cells were fixed,  
 8 permeabilized and immunostained for the endogenous lysosomal protein LAMP1. Nuclei were  
 9 labeled with DAPI (blue). Cell edges were outlined by staining of actin with fluorescent  
 10 phalloidin (not shown) and indicated by dashed lines. Scale bars: 20  $\mu$ m. **(F)** BORCS8-KO cells  
 11 were transiently transfected with the indicated HA-tagged constructs and immunostained for the  
 12 HA epitope and endogenous LAMP1 as described for panel **E**. **(G)** Schematic representation of  
 13 shell analysis.<sup>26</sup> **(H)** Quantification by shell analysis of peripheral LAMP1 signal in HeLa cells  
 14 from three experiments such as those shown in panels **E** and **F**. Data were represented as  
 15 SuperPlots<sup>45</sup> showing the individual data points, the mean from each experiment, and the mean  $\pm$   
 16 SD of the means. Statistical significance was calculated by one-way ANOVA followed by  
 17 multiple comparisons using Tukey's test. \* $p < 0.05$ ; \*\* $p < 0.01$ ; \*\*\*\* $p < 0.0001$ ; ns: not  
 18 significant.

19  
 20 **Figure 6 Zebrafish *borcs8* F0 KO larvae exhibit developmental defects.** **(A)** Morphology of  
 21 zebrafish WT, Cas9 control, and *borcs8* F0 KO larvae at 3 dpf. Scale bars: 1 mm. **(B)** Frequency  
 22 of phenotypes observed for WT, Cas9 control, *borcs8* F0 KO, and human *BORCS8* mRNA  
 23 rescue (Rescue) larvae (N=4, n=32-72). **(C-E)** Body length **(C)**, head size **(D)**, and eye size **(E)**  
 24 of WT, Cas9 control, *borcs8* F0 KO, and Rescue larvae at 3 dpf (N=3, n=8-9 for head size and  
 25 body length, n=16-18 for eye size). **(F)** H&E staining of paraffin-embedded brain sections from  
 26 the midbrain of 5-dpf WT and *borcs8* F0 KO larvae. Scale bar: 100  $\mu$ m. **(G)** Quantification of  
 27 brain size of *borcs8* F0 KO larvae (N=9) relative to WT (N=15) and Rescue (N=4) at 5 dpf. **(H)**  
 28 Phalloidin staining of muscles in *borcs8* F0 KO and WT larvae at 3 dpf. **(I,J)** Comparisons of  
 29 dorsal or ventral myotome area **(I)** and myoseptum angle **(J)** between WT (N=3, n=8) and  
 30 *borcs8* F0 KO larvae (N=3, n=8-9). All data are represented as the mean  $\pm$  SEM. Statistical

1 significance was calculated by one-way ANOVA followed by Tukey's multiple comparisons  
2 tests, or Student's t-test. \* $p < 0.05$ ; \*\* $p < 0.01$ ; \*\*\* $p < 0.001$ ; \*\*\*\* $p < 0.0001$ , ns: not significant.

3  
4 **Figure 7 Neuromuscular defects and impaired motility in *borcs8* F0 KO zebrafish larvae.**

5 **(A)** Primary motor axons in WT and *borcs8* F0 KO larvae at 3 dpf. Scale bars: 50  $\mu\text{m}$ . Defects in

6 axon branching are indicated by white arrows. **(B)** Quantification shows marked reduction in the

7 axon length of motor neurons in *borcs8* F0 KO (N=3, n=15) compared to WT (N=3, n=12) and

8 Rescue larvae (N=3, n=18). **(C)** Co-immunostaining of zebrafish NMJs with presynaptic (SV2;

9 green) and postsynaptic ( $\alpha$ -bungarotoxin; red) markers in 3 dpf zebrafish. Scale bars: 50  $\mu\text{m}$ . **(D)**

10 Quantification of colocalizing presynaptic and postsynaptic markers per hemisomite, normalized

11 to the number of presynaptic puncta, showed a significant reduction in the number of puncta in

12 *borcs8* F0 KO larvae (N=3-4, n=8-12). **(E)** Representative snapshots of touch escape responses

13 (N=6) over 350 milliseconds (ms). Zebrafish *borcs8* F0 KO larvae have very little to no escape

14 response at 2 dpf. **(F)** Representative swimming tracks of WT control and *borcs8* F0 KO fish at 5

15 dpf. The *borcs8* F0 KO larvae (N=3, n=32) displayed impaired swim distance and velocity

16 compared to controls (N=3, n=24). All data are represented as the mean  $\pm$  SEM. Statistical

17 significance was calculated by Student's t-test, or one-way ANOVA followed by Tukey's

18 multiple comparisons tests. \*\* $p < 0.01$ ; \*\*\* $p < 0.001$ ; \*\*\*\* $p < 0.0001$ , ns: not significant.

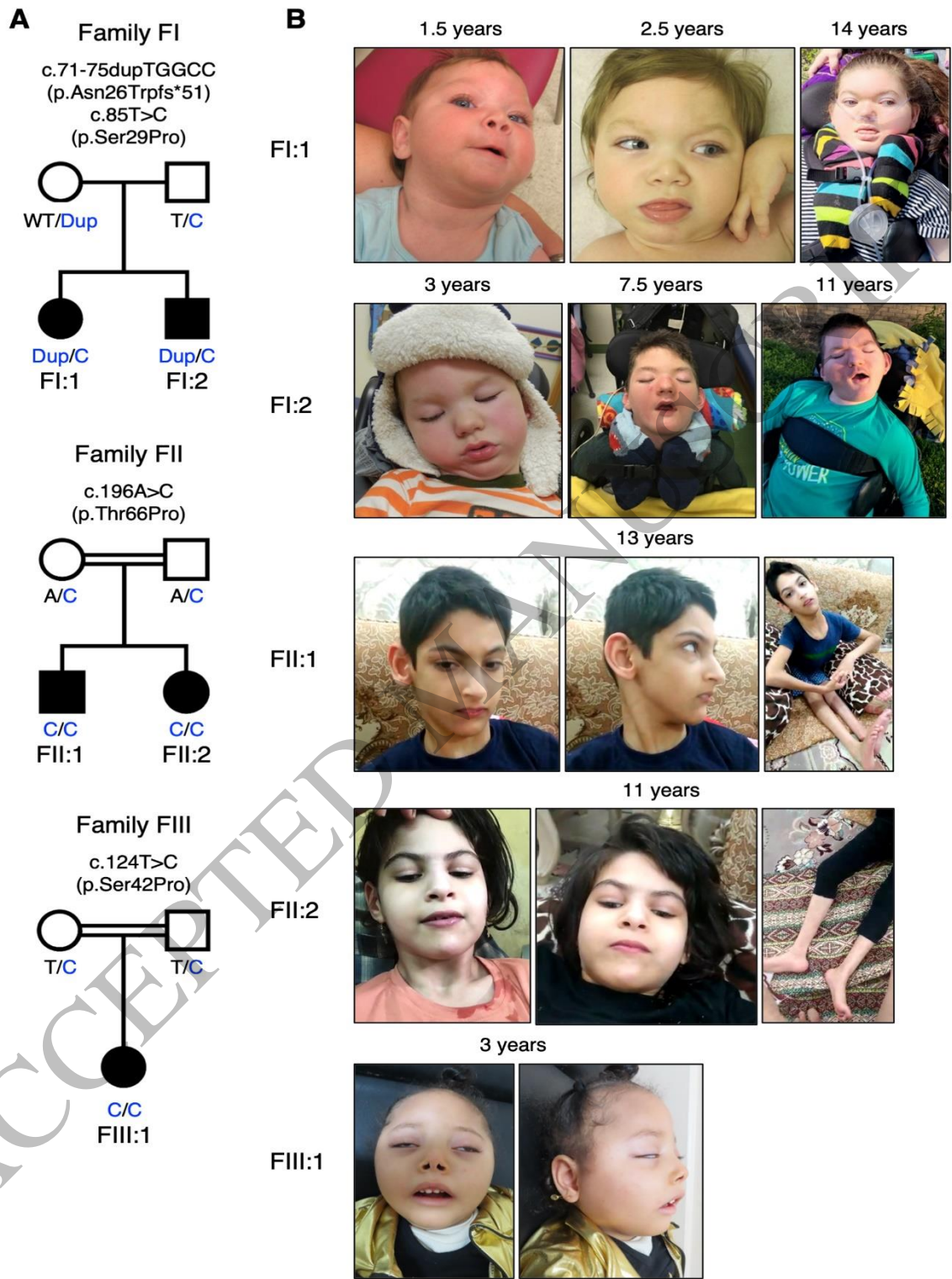


Figure 1  
 152x222 mm (x DPI)

1  
 2  
 3  
 4

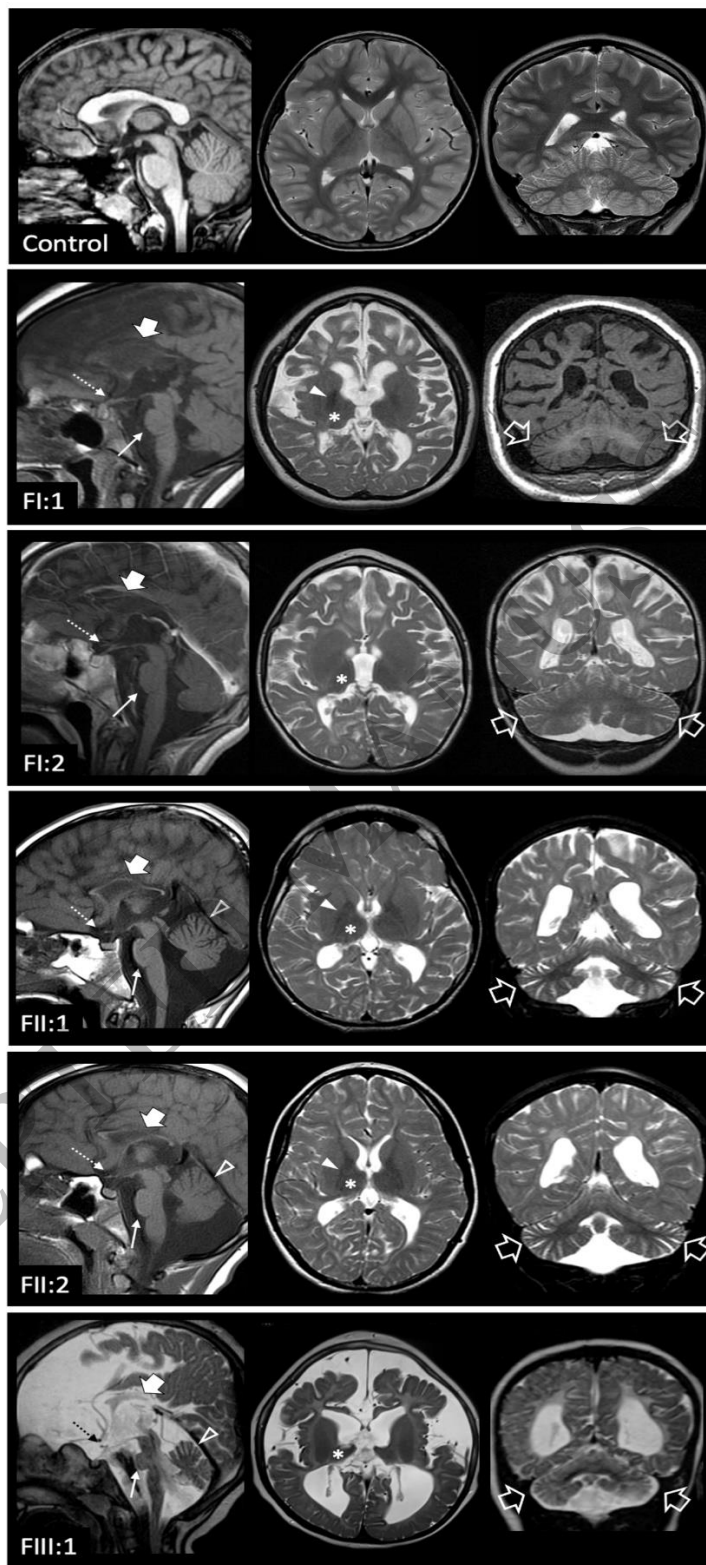


Figure 2  
95x244 mm (x DPI)

1  
2  
3  
4

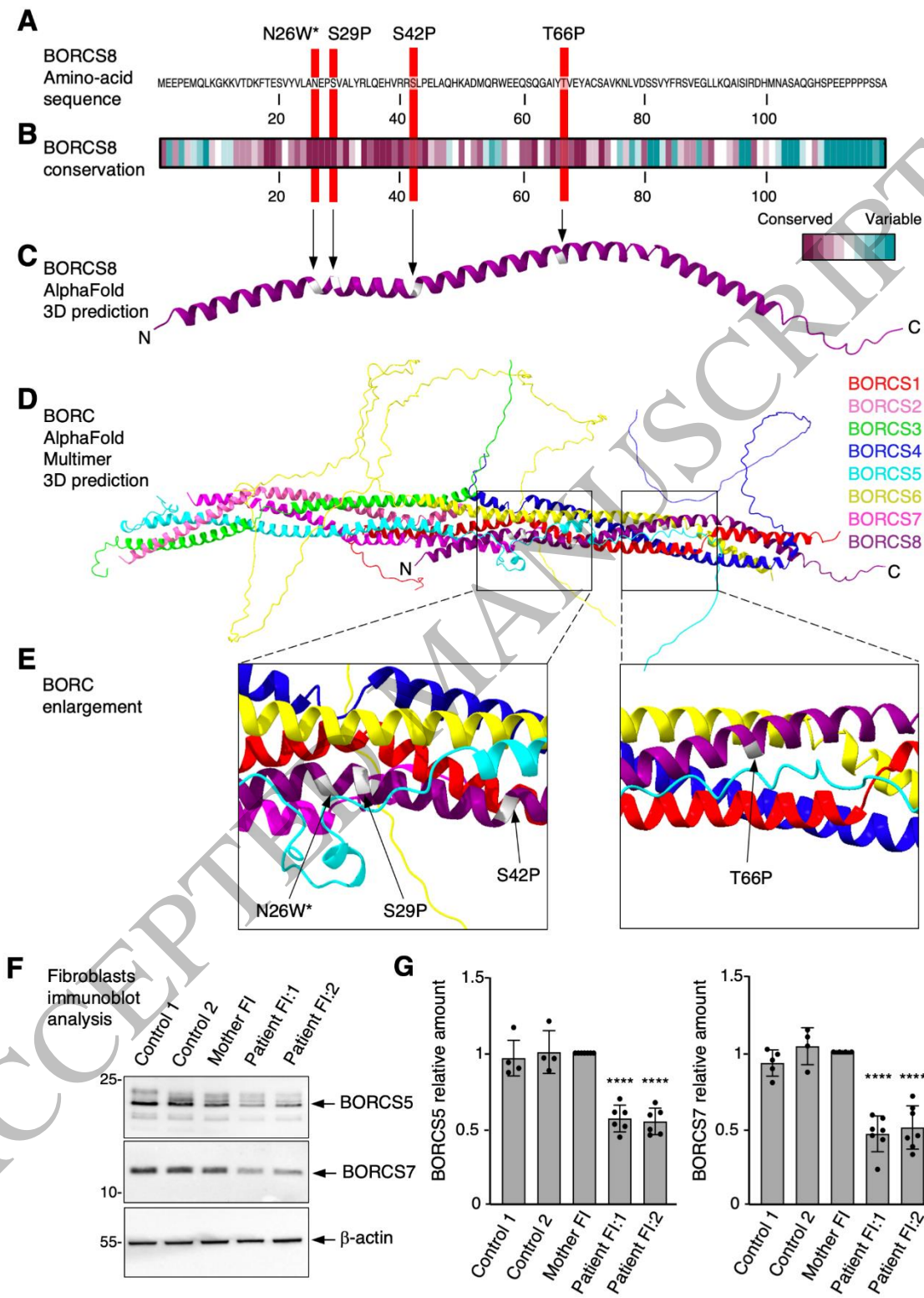


Figure 3  
151x210 mm (x DPI)

1  
2  
3

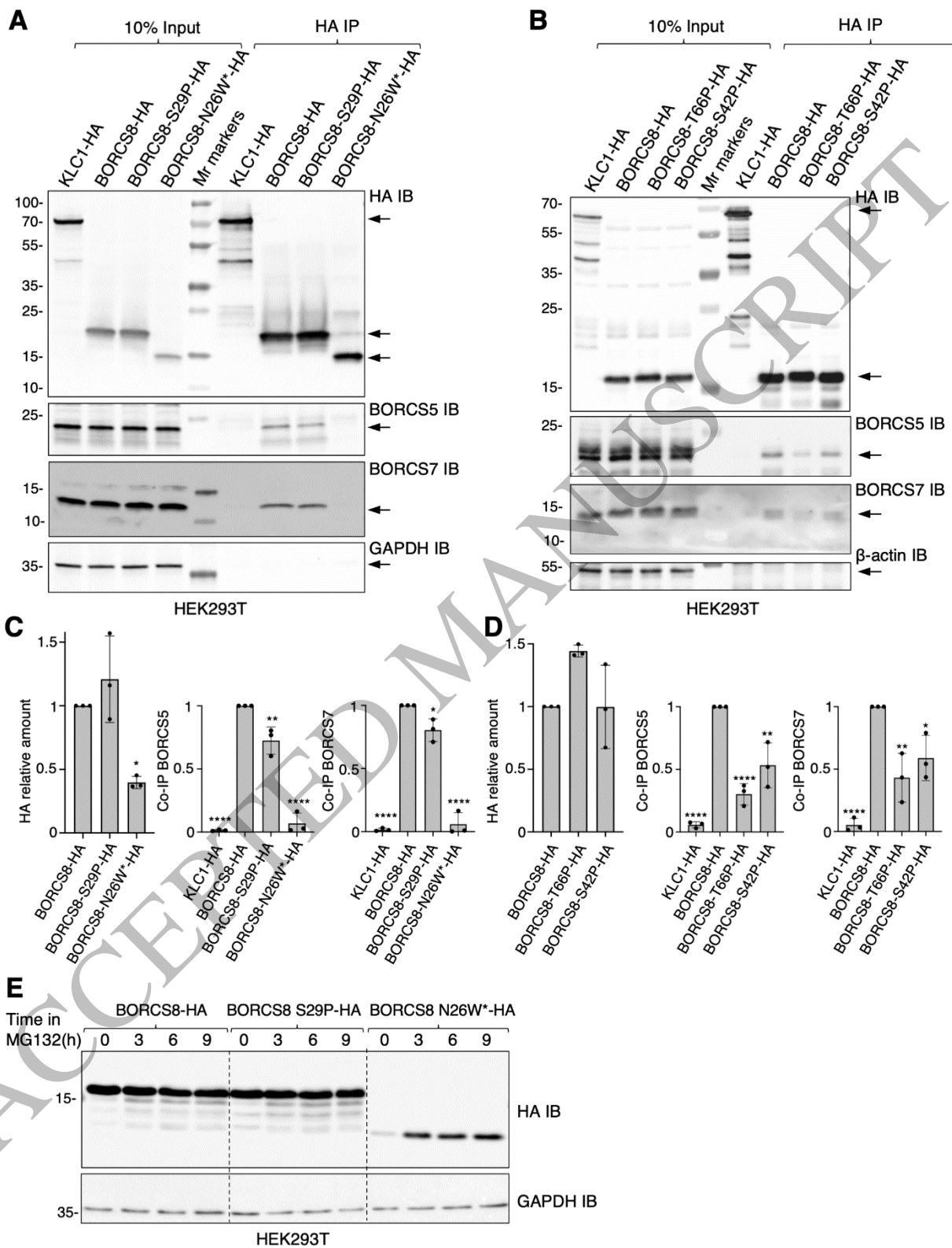


Figure 4  
166x213 mm (x DPI)

1  
2  
3

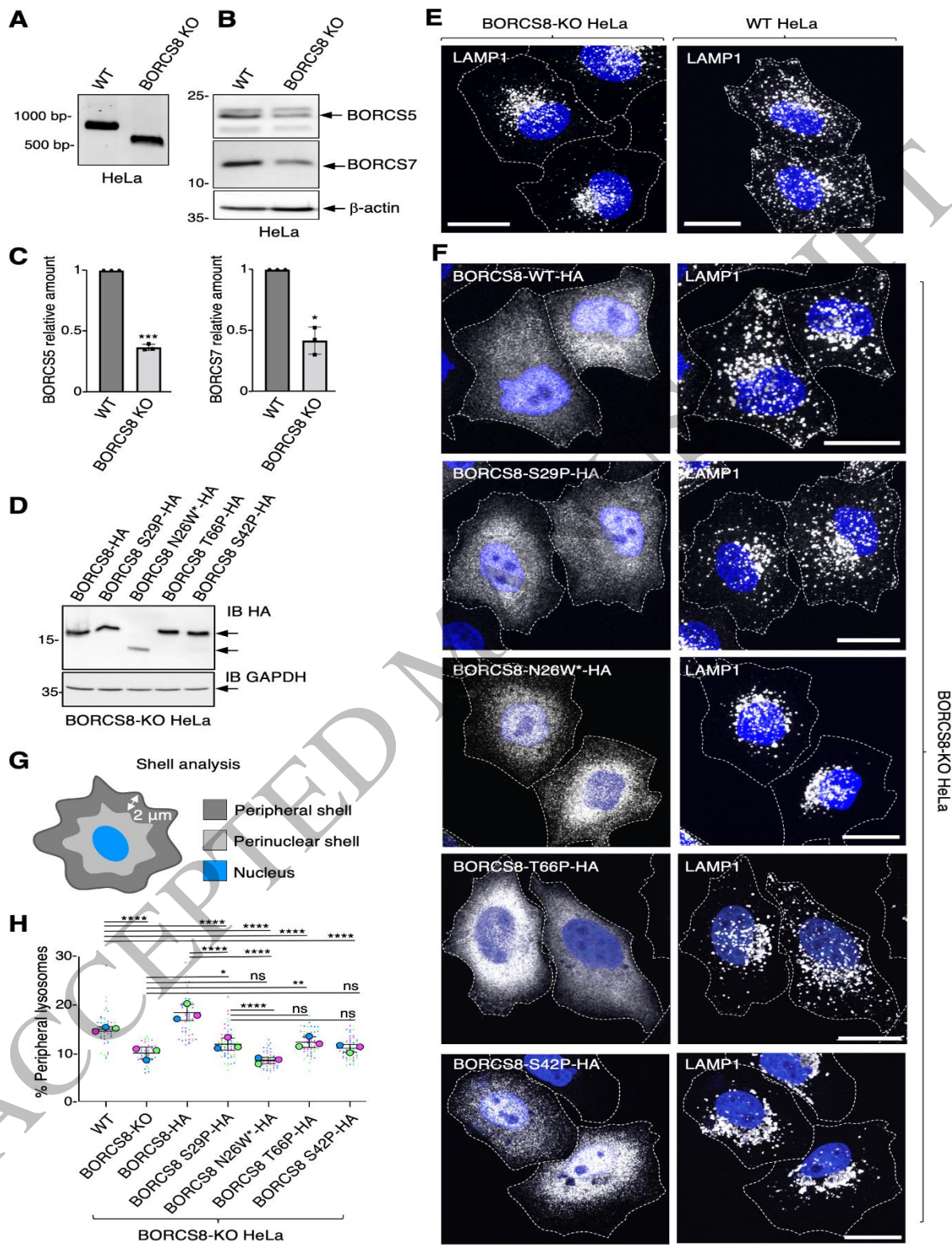


Figure 5  
161x251 mm (x DPI)

1  
2  
3  
4

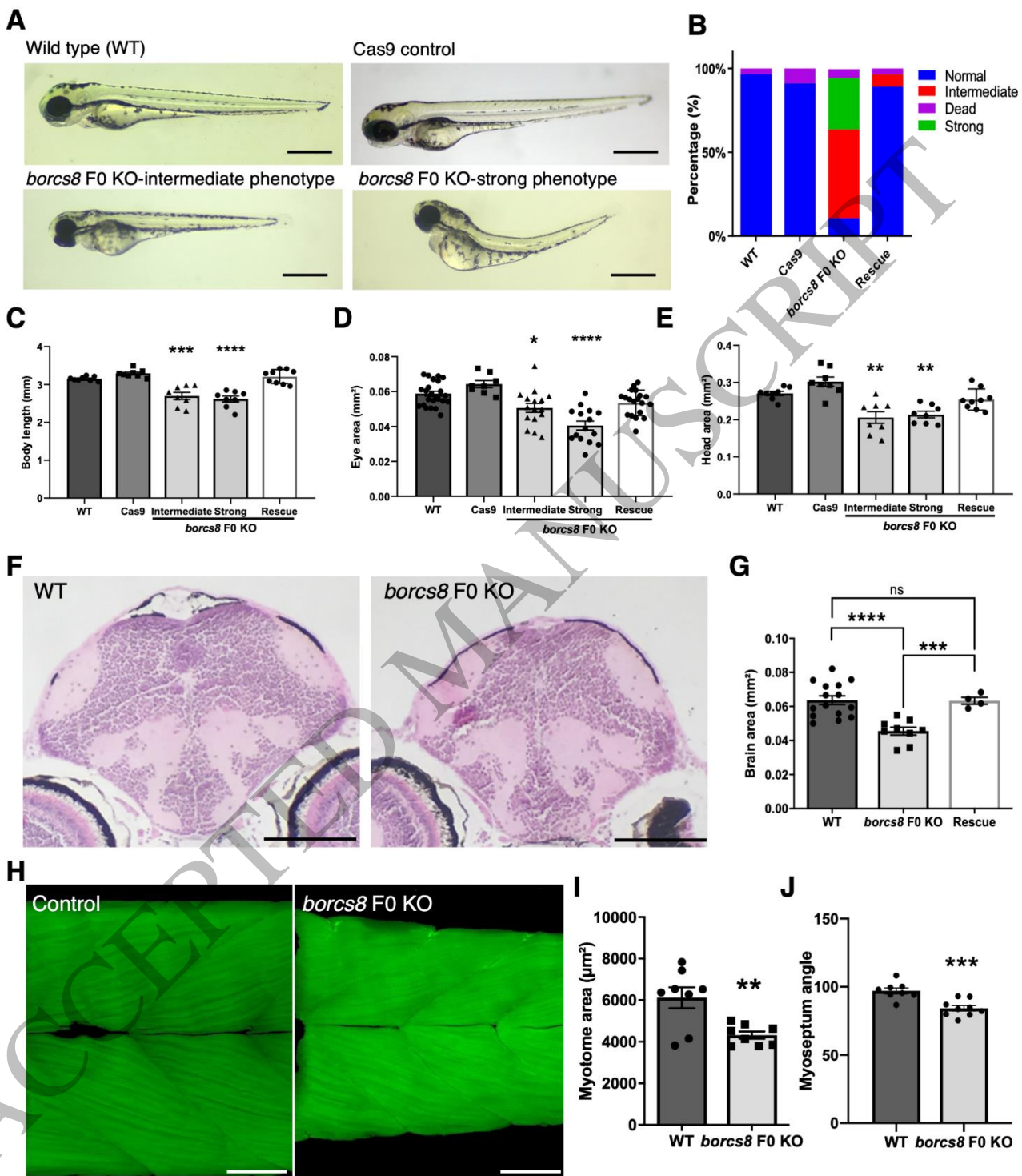


Figure 6  
174x198 mm (x DPI)

1  
2  
3  
4

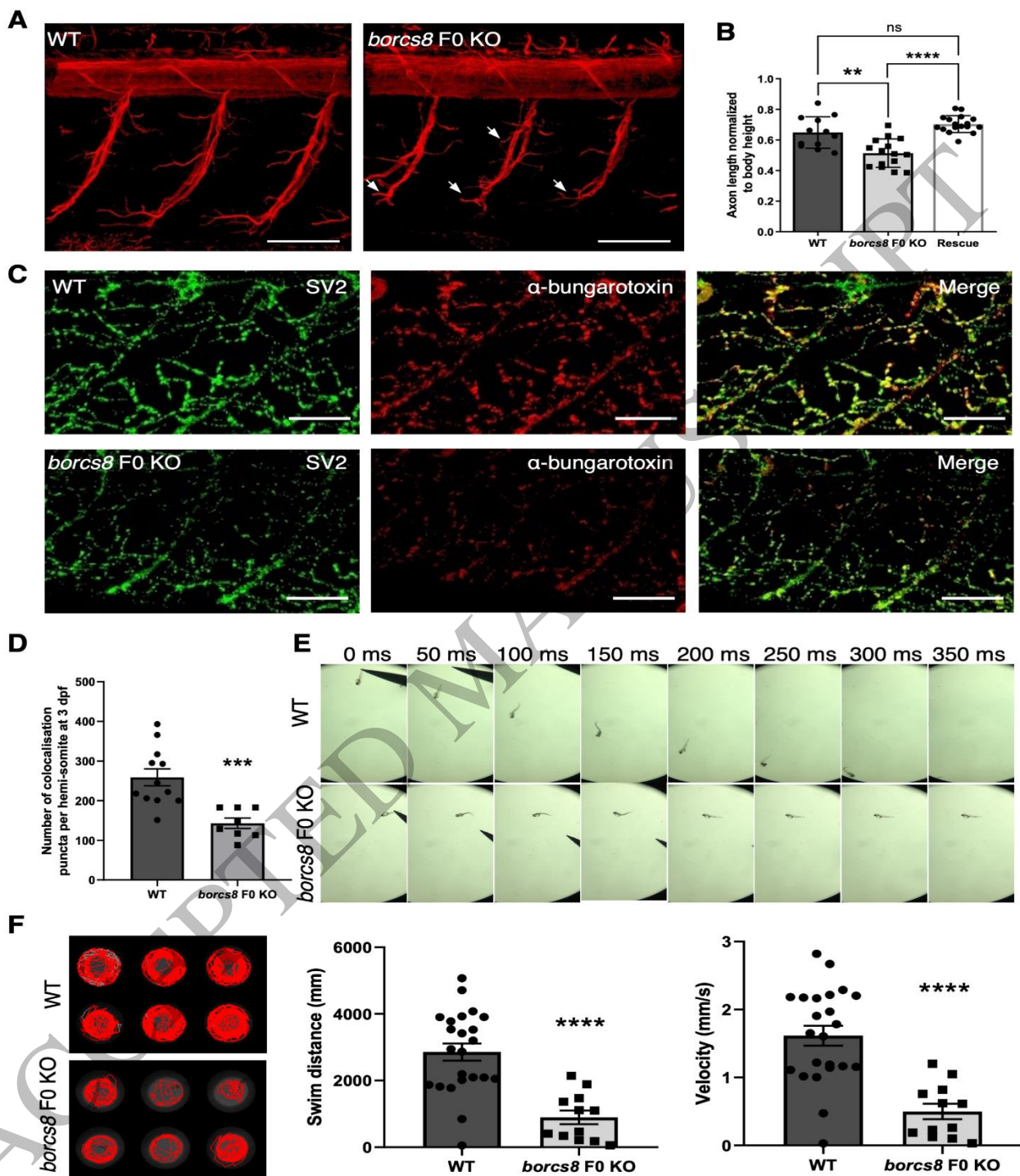


Figure 7  
169x224 mm (x DPI)

1  
2  
3  
4

1 **Table 1 Summary of genotypes and phenotypes of the BORCS8 variant patients**

Patients	FI:1	FI:2	FII:1	FII:2	FIII:1
Zygosity	Compound heterozygous	Compound heterozygous	Homozygous	Homozygous	Homozygous
Coding sequence changes	85T>C, 71-75dupTGGCC	85T>C, 71-75dupTGGCC	I96A>C	I96A>C	I24T>C
Amino-acid changes	Ser29Pro, Asn26Trpfs*51	Ser29Pro, Asn26Trpfs*51	Thr66Pro	Thr66Pro	Ser42Pro
Gender	Female	Male	Male	Female	Female
Ethnicity	European-American	European-American	Arab-Iranian	Arab-Iranian	Egyptian
Consanguinity	No	No	Yes	Yes	Yes
Age at last follow up	14 years	11 years	13 years	11 years	3 years
Hypotonia	Yes	Yes	Yes	Yes	Yes
Failure to thrive	Yes	Yes	Yes	Yes	Yes
Global developmental delay	Yes	Yes	Yes	Yes	Yes
Intellectual disability	Profound	Profound	Profound	Profound	Profound
Microcephaly	No	No	Yes	Yes	Yes
Hypotonia	Yes	Yes	Yes	Yes	Yes
Muscle weakness and atrophy	Yes	Yes	Yes	Yes	Yes
Seizures	Yes	Yes	No	No	Yes
Spasticity	Yes	Yes	Yes	Yes	No
Scoliosis	Yes	Yes	Yes	No	No
Dysmorphic features	Yes	Yes	Yes	Yes	Yes
Optic atrophy	Yes	Yes	Not assessed	Yes	Yes
Other clinical features	Restrictive lung disease, chronic respiratory disease, osteoporosis, G-tube dependency, impaired oropharyngeal motility, oral and pharyngeal dysphagia, hearing loss, urosepsis, chronic UTI	Chronic respiratory insufficiency, restrictive lung disease, chronic ear infections, osteoporosis, G-tube dependency, sensitive, dry skin	No	No	Recurrent chest infections due to aspiration, recurrent choking, feeding difficulties, bowel and urinary incontinence, sparse hair

2 For additional details, see Supplementary Table 1.